5 Dynamic current feedback control for fast torque impression in drive systems

The current control loop plays a decisive role in a 3-phase drive system operated with field orientation. The design of the superimposed mechanical systems (speed and position control) wishes for an inner *current control loop with ideal behaviour: With undelayed impression of the stator current*. The assumption that the ideal current control can be modeled by a dead time simplifies fundamentally the control design for often weekly damped oscillating mechanical systems.

Besides the dead time behaviour, which could be achieved by a design aimed at dead-beat response, the current controller also should ensure *an ideal decoupling between the field* and *torque forming components* i_{sd} and i_{sq}, because the two components are strongly coupled with each other in the field synchronous coordinate system. This problem was not solved convincingly with the classic concept (fig. 1.4). From the view of the modern control engineering the current process model of IM or PMSM represents a multivariable process – a MIMO[1] process – which can be mastered only by a multivariable controller. The multivariable controller contains besides controllers in the main (direct) path also cross (decoupling) controllers, so that the difficulties of the decoupling are solved automatically with the controller design.

An important task of the controller design consists in considering a number of implementation dependent issues in controller approach and feedback. With conventional PI controllers such issues are usually neglected.

- The delay of the control variable output of typically one sampling period: The stator voltage calculated by the current controller can only have an effect in the next sampling period.
- The technique of the actual-value measurement: After all, different possibilities like instant value measuring (by ADC) or integrating measuring (by VFC, resolver and incremental encoder) are considered.

[1] MIMO: Multi-Input – Multi-Output

Like all control equipment, the inverter can realize only a limited control variable because of the fixed DC-link voltage. To avoid possible oscillations and wind-up effects caused by the implicit integrating part after entering or leaving output limitation (at start-up, speed reversals, magnetization, field weakening), the controller must have the ability to take the limitation of control variables into account effectively.

After discussing the discrete system models in the former chapters, new controllers will now be introduced with uniform and easily comprehensible design and which fulfill all mentioned requirements. But before the controller design is discussed a survey about the existing current control methods shall be given.

5.1 Survey about existing current control methods

The interested reader will find an overview in abbreviated form also in [Quang 1990]. Altogether, the known methods can generally be divided into two groups: nonlinear and linear current controllers.

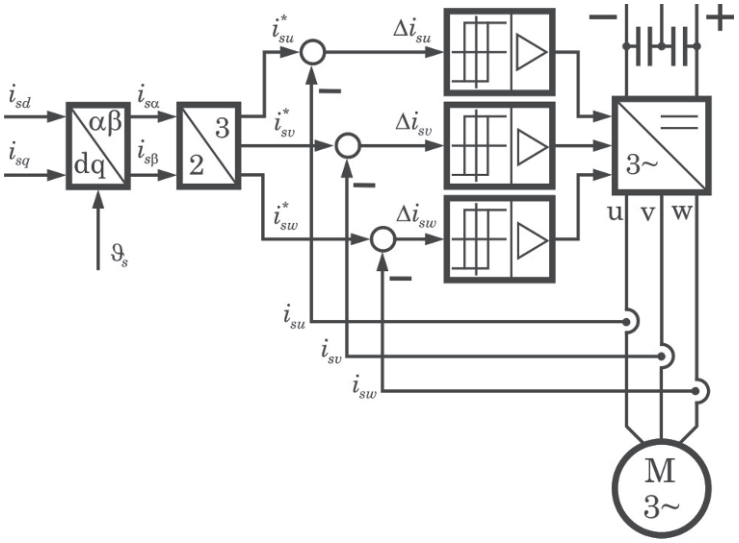

Fig. 5.1 Stator current control with three separate hysteresis (bang-bang) controllers

a) Nonlinear current control

Controllers of this group can show two- or three-point behaviour. A special method is the intelligent predictive control which reacts to the

stator current vector leaving a predefined tolerance circle with a pre-calculated optimal firing pulse and therefore has also two-point behaviour. The most simple version of a current controller with two-point behaviour is to use three separate on-off controllers, refer to [Peak 1982], [Pfaff 1983], [Hofmann 1984], [Brod 1985], [Le-Huy 1986], [Malesani 1987] and [Kazmierkowski 1988]. The principle is shown in the figure 5.1.

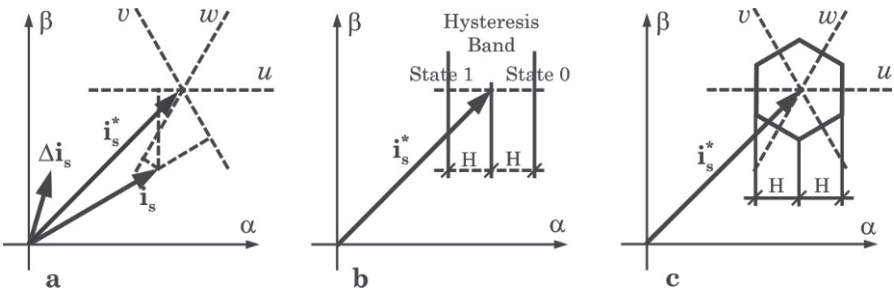

Fig. 5.2 On-off controller for phase currents in vector representation: Components of vector of current error (**a**), tolerance range of one phase (**b**) and tolerance hexagon of all three phases (**c**)

The sinusoidal set points of the phase currents are obtained by coordinate transformation from the field synchronous set points. Depending on the sign of the current errors, the corresponding phase is switched to „+“ or „–“ potential of the DC-link voltage at exceeding of the permitted error. This control variant stands out by the simplicity of its technical realization and by its convincing dynamic properties, but the following backdrops also have to be mentioned:

- The pulse frequency varies with changing fundamental frequency and load which is particularly unwanted.
- With isolated motor star point the current error can reach the double of the tolerance band.
- The control quality directly depends on analogous comparators which are sensitive to offset and drift and could therefore lead to a slight pre-magnetization of motor or transformer.

The figure 5.2a shows the reference vector of the stator current $\mathbf{i}_s^*$, the actual vector $\mathbf{i}_s$ and the error vector $\Delta \mathbf{i}_s$. The phase current differences are obtained by the projection of the error vector to the axes of the corresponding phase windings. Upon the actual current vector leaving the tolerance hexagon the comparators will become active.

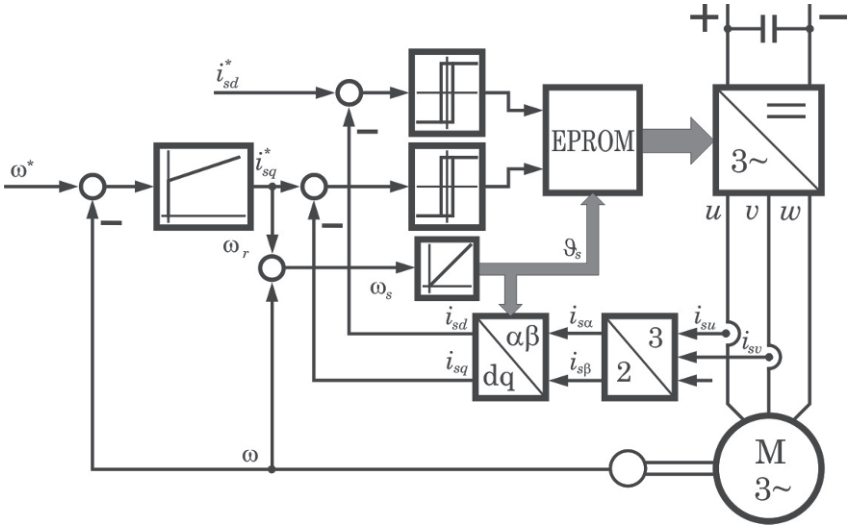

Fig. 5.3 Block structure of the drive system with inner current control loop using two-point controllers in field synchronous coordinates

The figure 5.3 shows the realization of the control with two-point behaviour in field synchronous coordinates (cf. [Pfaff 1983], [Nabae 1985], [Rodriguez 1987] and [Kazmierkowski 1988]). The current error is calculated in field synchronous coordinates. The field angle provides the necessary address to find, depending on the control errors, the fitting predefined pulse patterns. The figure 5.4 explains this.

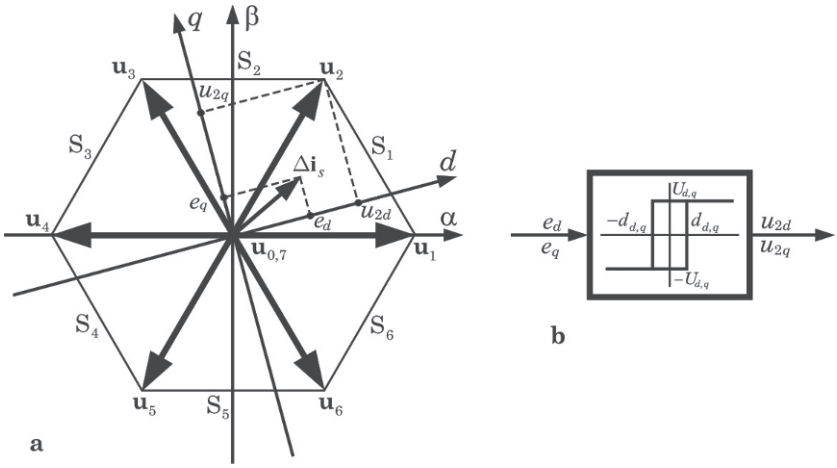

Fig. 5.4 Definition of the switching hysteresis in two-point current controllers in field synchronous coordinates

The actual error vector $\Delta\mathbf{i}_s$ and the position of the coordinate system are shown in figure 5.4a. Following the definition in figure 5.4b the controller behaviour can be summarized as follows:

$$\text{if } \varepsilon_{d,q} > \delta_{d,q}, \text{ then } u_{xd,xq} = U_{d,q} = 1 \text{ and}$$

$$\text{if } \varepsilon_{d,q} \le \delta_{d,q}, \text{ then } u_{xd,xq} = -U_{d,q} = 0$$

The values 1 and 0 are the logical values which are assigned to the voltages $\pm U_{d,q}$. Index "*x*" can assume one of the values 0...7 and represents the standard voltage vector to be selected. The projection of $\Delta\mathbf{i}_s = \mathbf{i}_s^* - \mathbf{i}_s$ to the axes *dq* like in the figure 5.4a yields:

$$\varepsilon_d > \delta_d \text{ , thus } u_{xd} = 1$$

$$\varepsilon_q > \delta_q \text{ , thus } u_{xq} = 1$$

Accordingly, a pulse pattern or a voltage vector has to be chosen whose *d* and *q* components minimize these control errors. In the example of figure 5.4 the choice $\mathbf{u}_2$ follows immediately. The assignment

logical values and position of field synchronous coordinate system $\rightarrow$ *firing pulse*

was determined off-line beforehand and then stored in table form in EPROM. [Rodriguez 1987] shows concrete examples.

To control the stator currents, also controllers with three-point behaviour may be used. In [Kazmierkowski 1988] details about this approach can be found which is illustrated in the figure 5.5. In this method the control errors ε_α and ε_β of the stator current are obtained by projection of the error vector to the $\alpha\beta$ axes of the stator-fixed coordinate system. The way to choose the required pulse pattern is similar as in the figure 5.3.

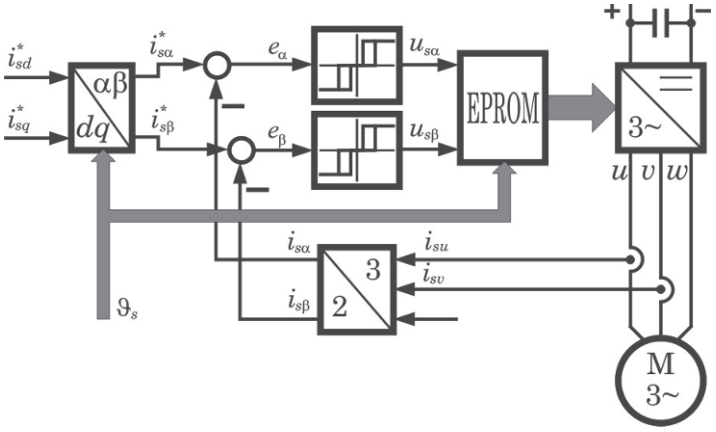

Fig. 5.5 Three-point current controller in stator-fixed coordinate system

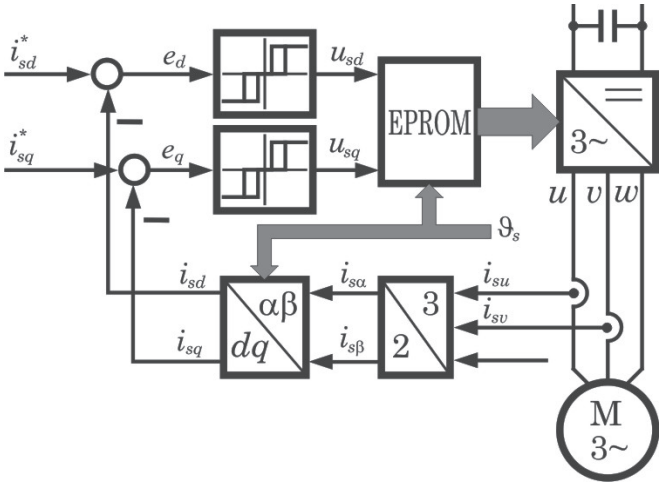

Fig. 5.6 Three-point current controller in field synchronous coordinate system

[Kazmierkowski 1988] further introduced a structure with three-point controllers in the field synchronous coordinate system as shown in the figure 5.6. In principle this variant works exactly like the one in figure 5.3. The only difference between both versions consists in aiming at a higher precision by a finer division of the overall vector space (figure 5.7) into 24 sectors, combined with three-point behaviour. The EPROM table containing the pulse patterns accordingly gets more extensive. In contrast, Rodriguez keeps the six original sectors (figure 5.4).

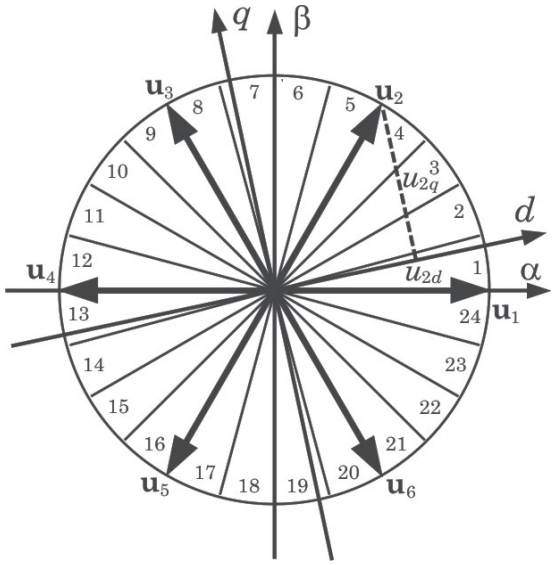

Fig. 5.7 Division of the vector space into 24 sectors

The most intelligent version in the family of the nonlinear current controllers is the predictive control (more in [Holtz 1983, 1985]). This control reacts (figure 5.8) on the actual current vector leaving the tolerance-circle by a predictive calculation of the following, optimized voltage vector. Therefore, it also shows two-point behaviour. The method can be used in field synchronous as well as in stator-fixed coordinates. The principle block structure is shown in the figure 5.9.

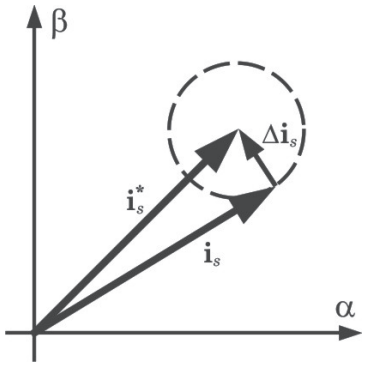

Fig. 5.8 Tolerance-circle of the predictive current controller

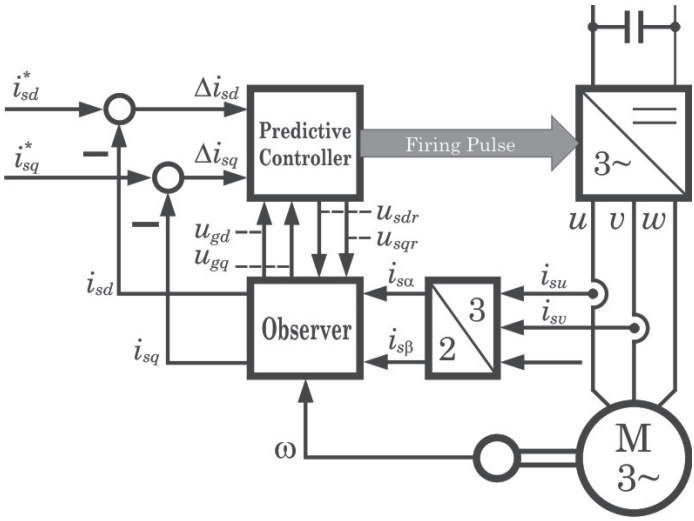

Fig. 5.9 Block structure of the predictive current control

If the actual vector $\mathbf{i}_s$ overlaps the tolerance-circle at the time t_0, the predictive controller must, using the information provided by the observer,

- calculate all possible trajectories of the current vector (figure 5.10a) for each of the seven possible standard voltage vectors, and
- following a certain criterion determine the optimal voltage vector for the chosen current trajectory.

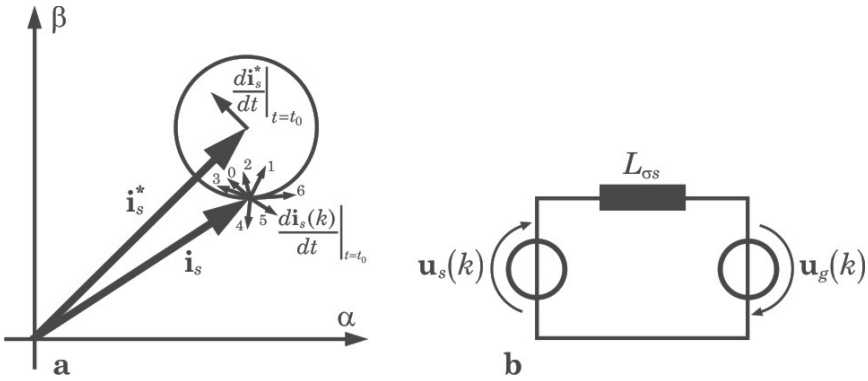

Fig. 5.10 Possible current trajectories on output of all possible standard voltage vectors (**a**) and simplified equivalent circuit of the IM (**b**)

The trajectories can be calculated as follows:

$$\begin{aligned}\mathbf{i}_s^*(t) &= \mathbf{i}_s^*(t_0) + \frac{d\mathbf{i}_s^*}{dt}\Big|_{t=t_0}(t-t_0)\\ \mathbf{i}_s(t) &= \mathbf{i}_s(t_0) + \frac{d\mathbf{i}_s}{dt}\Big|_{t=t_0}(t-t_0)\end{aligned} \tag{5.1}$$

In the equation (5.1) the currents $\mathbf{i}_s^*(t_0)$ and $\mathbf{i}_s(t_0)$ are known. The numerical derivation of $\mathbf{i}_s^*$ produces $d\mathbf{i}_s^*/dt$, and for calculation of $d\mathbf{i}_s/dt$ the following equation is used:

$$\frac{d\mathbf{i}_s(k)}{dt} \approx \frac{\mathbf{u}_s(k) - \mathbf{u}_g(t=t_0)}{L_{\sigma s}} \tag{5.2}$$

with:

k = 0, 1, ... , 7
$\mathbf{u}_s(k)$ = one of the seven possible standard voltage vectors
$\mathbf{u}_g(t=t_0)$ = the induced e.m.f. at instant t_0
$L_{\sigma s}$ = leakage inductance on the stator side

The formula (5.2) follows from the figure 5.10b in which the stator resistance is neglected. The induced e.m.f. is calculated by a machine model in the observer. Depending on the chosen trajectory (k = 0, 1, ... , 7) the following error vector:

$$\Delta\mathbf{i}_s(t,k) = \mathbf{i}_s^*(t) - \mathbf{i}_s(t,k) \tag{5.3}$$

can be calculated. For a detailed derivation the interested reader is referred to the mentioned literature. Here only the final equation (5.4), which shows the different error trajectories (figure 5.10c) in dependency on the chosen voltage vectors, is given.

$$\left|\Delta\mathbf{i}_s\right|^2(t,k)=\left|\Delta\mathbf{i}_s\right|^2(t=t_0)+a_1(t-t_0)+a_2(t-t_0)^2 \tag{5.4}$$

The error trajectories have the form of a parabola. From the figures 5.10a and 5.10c it can be seen, that the firing pulses corresponding to the voltage vectors $\mathbf{u}_4$ and $\mathbf{u}_5$ would increase the error, while all others would decrease it.

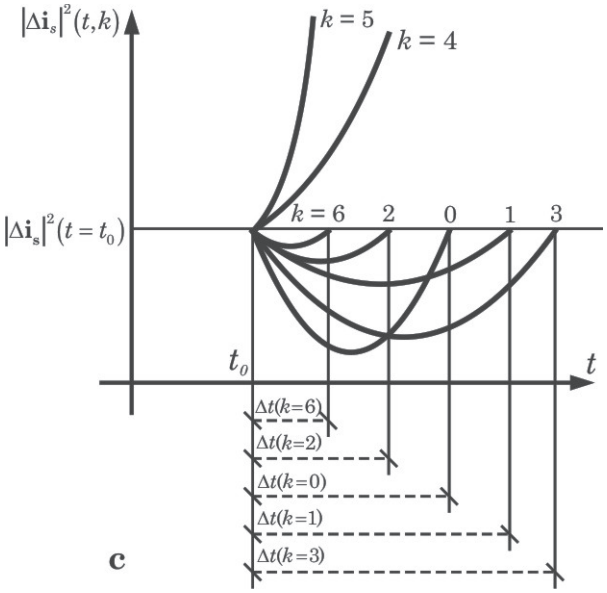

Fig. 5.10c Possible current trajectories at instant t_0

But naturally only one of the five vectors $\mathbf{u}_{0,1,2,3,6}$ can be used. The choice is made according to one of the following criteria:

1. For slow change of current (stationary operation): In this case the actual vector has to be kept within the tolerance circle as long as possible. In addition, the number of necessary switchovers of the semiconductor switches should be as small as possible. Therefore the following criterion is appropriate:
$$\frac{\Delta t(k)}{n(k)}=\max \tag{5.5}$$
2. For fast change of current (dynamic operation): This case produces very fast changes of the set point vector $\mathbf{i}_s^*$, and it requires that the actual vector $\mathbf{i}_s$ follows the set point vector exactly and as fast as possible. $\mathbf{u}_s(k)$ will then be chosen according to the following criterion:
$$\Delta t(k)=\min \tag{5.6}$$

For the example in figure 5.10c, using the first criterion would result in choosing vectors $\mathbf{u}_1$ or $\mathbf{u}_3$, whereas the second criterion yields vector $\mathbf{u}_6$.

The predictive control is predominantly used in high power drives, where the assumption of a negligible stator resistance is fulfilled widely and where a very large rotor time constant allows the choice of a relatively large sampling period, what is necessary because of the extensive required calculations.

The disadvantage of all nonlinear current control methods consists in the bad current impression in the area of inverter over-modulation, resulting in a certain orientation error and corresponding torque deviation.

b) Linear current control

Relevant references for this method are [Mayer 1988], [Meshkat 1984], [Rowan 1987] and [Seifert 1986]. The first classical version of linear current controllers was the application of three or two separate PI-controllers to independently control the phase currents (see fig. 5.11). The sinusoidal output signals of the PI controllers would be forwarded to pulse width modulators (PWM) and compared with a sawtooth-shaped pulse sequence. The firing pulses are the immediate result of this comparison.

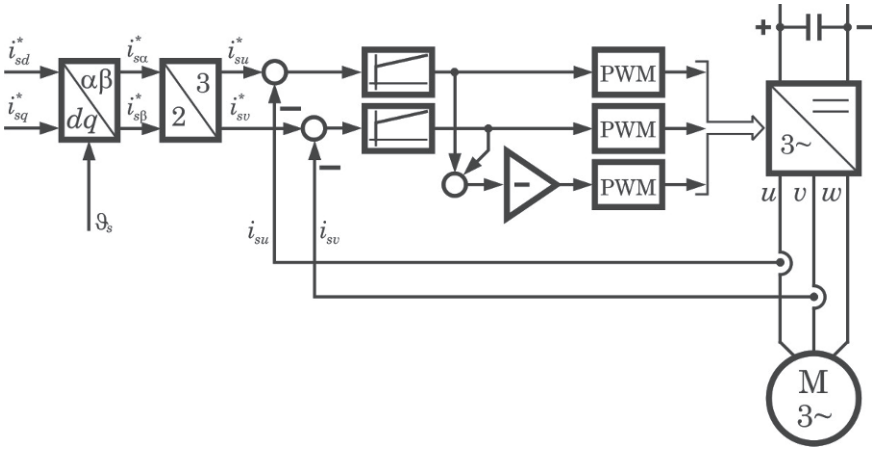

Fig. 5.11 Phase current PI controllers with pulse width modulation

The pulse width modulation was for long time the most widely used control method for inverters. Like all methods in stator-fixed coordinates, the control method shown in the figure 5.11 has the tracking error as a main disadvantage, because the PI controllers permanently have to work in dynamic operation due to the sinusoidal current set points. It was shown by [Rowan 1987] that an *abrupt reduction of the PWM gain* arises if the inverter control goes close to the maximum voltage amplitude (transition mode). This effect of the control variable limitation could not be taken into

account effectively with this control method. An essential improvement could be obtained by transforming the control algorithm into the field synchronous coordinate system (figure 1.4) in which the variables to be controlled represent DC quantities in stationary operation.

This control version is very widely applied and possesses the following advantages:

1. The precision is considerably higher because the controller does not have to work in dynamic operation, particularly the current phase error can be controlled to zero.
2. The response near the transition mode is improved.
3. The decoupling of the current components is improved, and therefore a higher accuracy of the field orientation is obtained.

This method however still has a number of disadvantages which shall be mentioned here to motivate the development of improved algorithms in the following chapters.

1. The response time (or the dynamics) of the control strongly depends on the stator leakage time constant. Therefore, a nearly undelayed current or torque impression as ideally required by the speed control loop is hardly achievable.
2. The current components i_{sd} and i_{sq} are strongly coupled to each other in field synchronous coordinates. Can an adequate decoupling be ensured?
3. Can the transfer characteristic of the current measuring technique actually used (measurement of instantaneous values, integrating measurement) be taken into account with this control concept effectively to guarantee a wide application range?
4. Can the one-step delay of the control variable $\mathbf{u}_s$, calculated by PI controllers, effectively be integrated into the control equations?
5. How does the controller react to the control variable limitation, and can switching-off of the integral part (anti-reset wind up) be regarded as a sufficient method in the PI controllers?

These questions will be answered in context with new designs of the current controller in this chapter. However, it has already to be highlighted that this variant represented a considerable progress to formerly applied methods.

A last method shall be mentioned yet, being a mixture between a linear and nonlinear regulation. This is the method introduced in [Enjeti 1988] and [Zhang 1988] with current modulus and current phase control (fig. 5.12a). The current modulus and current phase control loops are designed separately and have in principle linear characteristics. The decoupling of the two quantities, however, is of nonlinear nature. The references and the actual values are rectified and then compared with each other. The current

deviation is supplied to a PI controller. The phase angles are determined and compared with each other by phase detectors. The phase deviation has the form of a time interval during which a counter counts. The output of the A/D converter, following the PI modulus controller, and the output of the phase counter then build the address word for the corresponding switching pattern stored in a 64 Kbytes EPROM table.

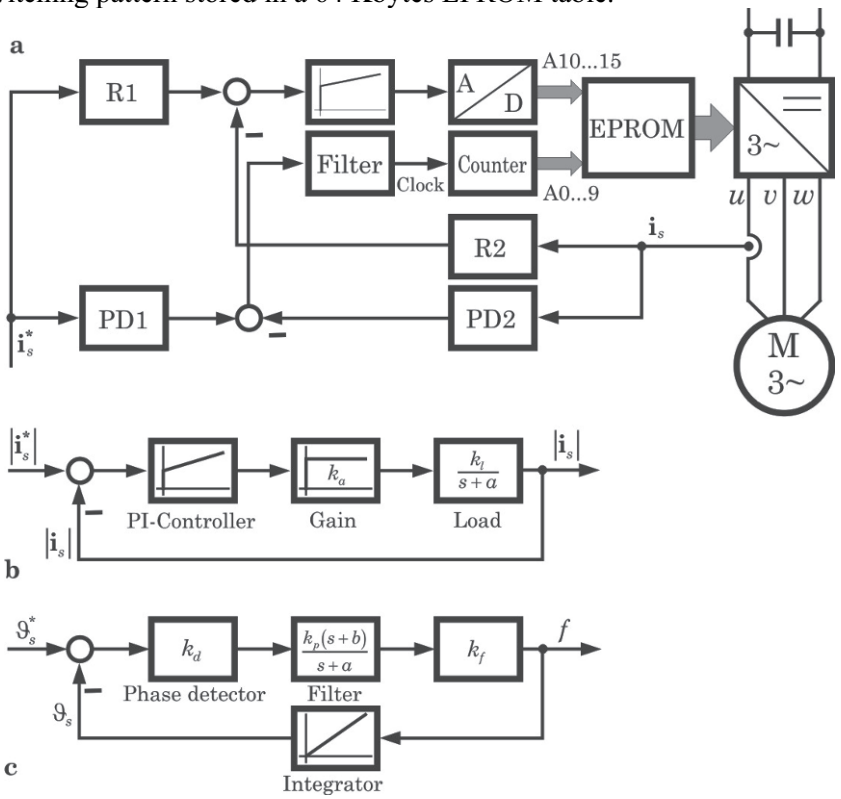

Fig. 5.12 Structure of the concept using current modulus and current phase control (**a**): the modulus control loop (**b**) and the phase or frequency control loop (**c**)

This control concept is mainly used in current source inverters with the control system designed according to the signal diagrams shown in figure 5.12b,c (see [Enjeti 1988]).

c) Closing remark to the overview

This chapter tried to give a summary of the known current control methods. Where possible, the functional principle was outlined. In connection with this, reference sources are included so that the possibility for background investigation is always ensured.

Because of the wide variety of the known methods deviations to the originals are conceivable. The aim of this summary was not to deliver a complete analysis about all methods, but rather to give a stimulus for own study.

5.2 Environmental conditions, closed loop transfer function and control approach

The consideration of all environmental conditions is one of the most important tasks of the controller design. Before the controller approach itself is developed these conditions shall be discussed here. In addition, the final closed loop behaviour to be achieved shall also be outlined.

a) Environmental conditions

The first condition to be considered is the *applied technique for capturing the actual-values of current and speed.* Basically, two main techniques exist: The measurement of instantaneous values using A/D converters, and the integrating measurement using V/f converters for the current and incremental encoder or resolver for the speed. The difficulties connected to this were discussed extensively in the chapter 4, but how they influence the controller design will be subject of this chapter 5.

The second environmental condition is the *one-step delayed output of the control variable* $\mathbf{u}_s$ of the current controller. This delay must be taken into account in the controller approach.

The rotor flux of the IM is, in comparison to other electrical quantities, a slowly changing variable. The pole flux of the PMSM is constant. Therefore the fluxes can be looked at as disturbance variables and shall be accounted for in the controller approach separately.

c) Closed loop response

The closed loop response is the intended transfer behaviour of the controlled system. In the case of the stator current controller, it is characterized by the following properties:

1. The step rise time, characterizing the control dynamics, and
2. the decoupling between the components in steady-state and dynamic operation.

The ideal dynamic behaviour can be achieved by the so-called *dead beat response* which means that the actual value will match the reference value after one sampling period, or, if the one-step delay of the control output is taken into account, after two sampling periods. Considering that for some

systems working with very short sampling times (e.g. T = 100µs) this rise time of 2×100µs would be too small from the viewpoint of the required energy to drive the current, a rise time of 3×100µs or 4×100µs (meaning after three or four periods) could be more useful in these cases. The dynamics does not become worse because a rise time of 300µs or 400µs (still much smaller then 1ms) can only be wished for with conventional PI controllers. To be able to express the demanded behaviour in general terms we start from a closed loop response with *n* sampling periods (figure 5.13) for the SISO process.

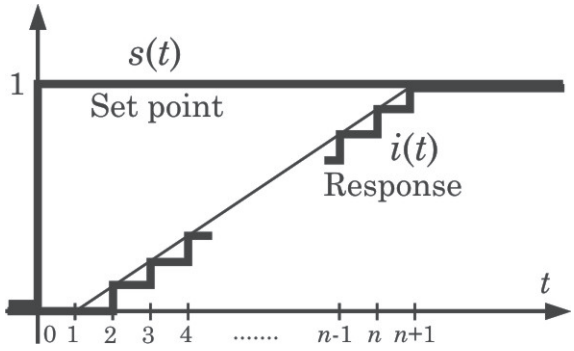

Fig. 5.13 Set point signal and its response of a SISO process controlled with dead-beat behaviour

The discrete control by means of micro computer allows for an exact tracking of the actual value so that it can reach the set point after *n* sampling periods exactly and without overshots. Such a controller is conceived, as well known, for *finite adjustment time* (FAT response). Considering the one-step delay of the control variable the FAT will then be exact (*n*+1) periods. Therefore, the approach for the output signal can be written in the z domain as follows (figure 5.13):

$$i(z)=\sum_{\nu=0}^{\infty} c_\nu\, z^{-\nu} \quad \text{with} \quad \begin{cases} c_0 = 0 \\ c_1 ... c_n = c_k = \dfrac{k-1}{n} \quad (k = 1 ... n) \\ c_{n+1} = c_{n+2} = ... = c_\infty = 1 \end{cases} \tag{5.7}$$

With $z < 1$ it can be obtained:

$$i(z)=\frac{z^{-(n+1)}}{1-z^{-1}}+\sum_{\nu=1}^{n}\frac{\nu-1}{n}z^{-\nu} \tag{5.8}$$

If a step change of the set point

$$s(z)=\frac{1}{1-z^{-1}} \tag{5.9}$$

is considered as characteristical excitation signal the general transfer function is obtained as:

$$i(z)=\left[z^{-(n+1)}+\left(1-z^{-1}\right)\sum_{\nu=1}^{n}\frac{\nu-1}{n}z^{-\nu}\right]s(z) \tag{5.10}$$

for the controlled SISO process with FAT response (figure 5.13). The closed loop response of the vectorial stator current control is obtained from equation (5.10) to:

$$\mathbf{i}_s(z)=\left[z^{-(n+1)}+\left(1-z^{-1}\right)\sum_{\nu=1}^{n}\frac{\nu-1}{n}z^{-\nu}\right]\mathbf{i}_s^*(z) \tag{5.11}$$

The closed loop response (5.11) means,

1. that the dynamic as well as the static decoupling between the current components i_{sd} and i_{sq} will be guaranteed, because the transfer matrix is the unity matrix or a diagonal matrix respectively, and
2. that the FAT response with FAT = (n+1) sampling periods will result for the decoupled current components.

It will be shown later that a FAT response with a higher step number is always connected with a complete change of the controller structure or with an increased computing time. It is therefore impractical to increase the number of steps exaggeratedly. The investigation has shown that a FAT response with FAT = 2, 3 or 4 periods, referring to the computation effort which must be handled during a very short sampling period (e.g. 100...200µs), would be realistic and practicable. Therefore, only controller designs for these three cases are offered later on. The reference transfer functions or the closed loop response are obtained as follows for:

1. n=1: FAT = n+1 = 2 (dead beat behaviour)

$$\mathbf{i}_s(z)=z^{-2}\,\mathbf{i}_s^*(z) \tag{5.12}$$

2. n=2: FAT = n+1 = 3

$$\mathbf{i}_s(z)=\frac{1}{2}\left(z^{-2}+z^{-3}\right)\mathbf{i}_s^*(z) \tag{5.13}$$

3. n=3: FAT = n+1 = 4

$$\mathbf{i}_s(z)=\frac{1}{3}\left(z^{-2}+z^{-3}+z^{-4}\right)\mathbf{i}_s^*(z) \tag{5.14}$$

c) Controller approach

It was tried in the subchapter 3.5 to agree on a common representation for the current control processes for IM and PMSM, resulting in the general process models (3.86) or (3.87) and the block structure in the figure 3.16. The equations represent the control process both in the field synchronous and in the stator fixed coordinate system. They are repeated here in favor of a better overview.

$$\mathbf{i}_s(k+1) = \mathbf{\Phi}\,\mathbf{i}_s(k) + \mathbf{H}\,\mathbf{u}_s(k) + \mathbf{h}\,\psi(k) \tag{5.15}$$

In z domain:

$$z\,\mathbf{i}_s(z) = \mathbf{\Phi}\,\mathbf{i}_s(z) + \mathbf{H}\,\mathbf{u}_s(z) + \mathbf{h}\,\psi(z) \tag{5.16}$$

Using these equations the controller design shall be carried out first in general and then applied for concrete cases. Under the assumption that **y** is the actual controller output quantity the following general controller approach arises.

$$\begin{aligned} \mathbf{u}_s(k) &= \mathbf{H}^{-1}\left[\mathbf{y}(k-1) - \mathbf{h}\,\psi(k)\right] \quad \text{or} \\ \mathbf{u}_s(k+1) &= \mathbf{H}^{-1}\left[\mathbf{y}(k) - \mathbf{h}\,\psi(k+1)\right] \end{aligned} \tag{5.17}$$

The term **y**(k-1) takes into account by the time shift (k-1), that in the current calculation the value of the controller output quantity **y** calculated in the period before is used. With that the one-step delayed output of the control variable is included in the approach. The 2nd term with $-\mathbf{h}\,\psi(k)$ compensates the flux dependent part. After inserting equation (5.17) into the equation (5.15) this immediately becomes recognizable, and the compensated general current process model (5.18) arises for the IM as well as the PMSM:

$$\mathbf{i}_s(k+1) = \mathbf{\Phi}\,\mathbf{i}_s(k) + \mathbf{y}(k-1) \tag{5.18}$$

In the z domain the following equation holds:

$$\left[z\,\mathbf{I} - \mathbf{\Phi}\right]\mathbf{i}_s(z) = z^{-1}\,\mathbf{y}(z) \tag{5.19}$$

The figure 5.14 illustrates the compensated current process model which serves as a starting point subsequently for all controller designs. In the following the methodical procedure will always be to address the general design first. After that the design will be specified to the concrete case: IM or PMSM, in field synchronous or in stator fixed coordinates. For this purpose the designs are always represented both in the form of equations and by circuit diagrams so that programming will be made easier.

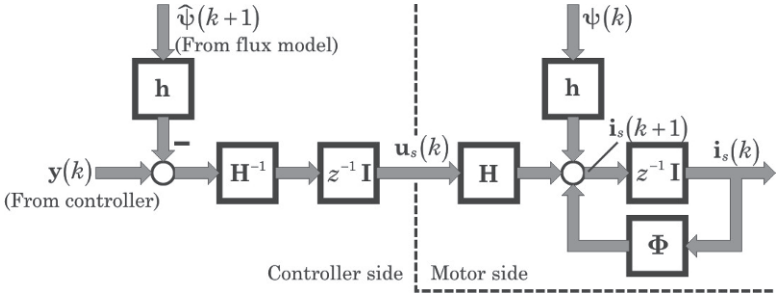

Fig. 5.14 General compensated current process model of the IM and PMSM

5.3 Design of a current vector controller with dead-beat behaviour

The designs in this chapter were introduced repeatedly in different papers [Quang 1991, 1993 and 1996].

5.3.1 Design of a current vector controller with dead-beat behaviour with instantaneous value measurement of the current actual-values

The figure 5.15 shows the principle block structure of the current vector controller with instantaneous value measurement for the example of the measuring strategy in figure 4.1. The controller equation is for this case:

$$\mathbf{y}(z) = \mathbf{R_I}\left[\mathbf{i}_s^*(z) - \mathbf{i}_s(z)\right] \tag{5.20}$$

$\mathbf{i}_s^*(z)$ = Reference or set point vector of the current

After substituting equation (5.20) into the equation (5.19) the following transfer function of the current controlled IM or PMSM can be obtained:

$$\mathbf{i}_s(z) = z^{-1}\left[z\mathbf{I} - \mathbf{\Phi} + z^{-1}\mathbf{R_I}\right]^{-1}\mathbf{R_I}\,\mathbf{i}_s^*(z) \tag{5.21}$$

The approach (5.12) is valid for the closed loop response and respectively for the reference transfer function. The equation (5.12) will be identical with (5.21), if the following equation holds for $\mathbf{R}_\mathrm{I}$:

$$\mathbf{R_I} = \frac{\mathbf{I} - z^{-1}\mathbf{\Phi}}{1 - z^{-2}} \tag{5.22}$$

The transfer function (5.12) illustrates by the diagonal matrix whose elements are z^{-2} a both statically and dynamically good decoupling between the current components. The controller $\mathbf{R}_\mathrm{I}$ (5.22) in figure 5.15 shows that a decoupling network in the classical presentation (figure 1.4) can be abandoned.

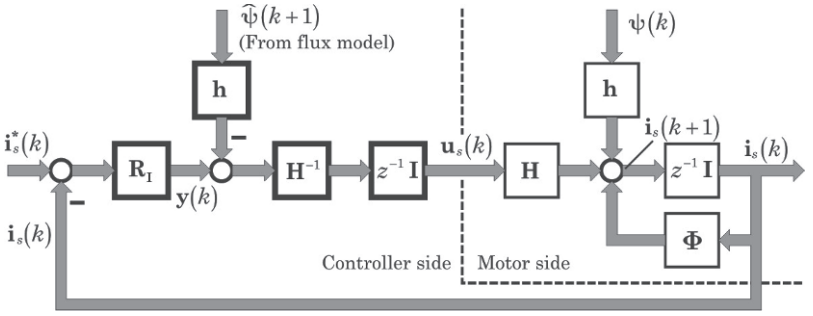

Fig. 5.15 Block structure of the current vector controller for IM or PMSM

With the current control error:

$$\mathbf{x}_w(z) = \mathbf{i}_s^*(z) - \mathbf{i}_s(z) \tag{5.23}$$

it will be obtained:

$$\mathbf{y}(z) = \mathbf{R_I}\,\mathbf{x}_w(z) \tag{5.24}$$

In the time domain the following controller equation results from equation (5.22):

$$\mathbf{y}(k) = \mathbf{x}_w(k) - \boldsymbol{\Phi}\,\mathbf{x}_w(k-1) + \mathbf{y}(k-2) \tag{5.25}$$

After inserting equation (5.25) into the equation (5.17) the control variable and respectively the stator voltage, which must be applied on the motor by the vector modulation, is obtained.

$$\mathbf{u}_s(k+1) = \mathbf{H}^{-1}\left[\mathbf{x}_w(k) - \boldsymbol{\Phi}\,\mathbf{x}_w(k-1) + \mathbf{y}(k-2) - \mathbf{h}\,\widehat{\psi}(k+1)\right] \tag{5.26}$$

With the equation (5.26) the design is complete. Two notes, however, are still necessary here.

1. The estimated rotor flux $\widehat{\psi}(k+1)$ (by equations 3.51, 3.55; in detail cf. subchapter 4.4) is used to compensate its disturbance effect. It is constant in the constant flux area and perhaps can be neglected in the practical implementation. The implicit I part in the controller is able to compensate for the missing flux compensation. However, the slowly variable flux in the field weakening area is exposed to permanent changes. It is therefore more advantageous to include the compensation into the equation (5.26).
2. The voltage or the control variable $\mathbf{u}_s$ will be calculated by processing the equation (5.26) always one sampling period ahead. With that the delay of the control variable $\mathbf{u}_s$ by one sampling period is taken into account.

a) Use of the controller for the IM in field synchronous coordinates

To be able to use the design (5.22) and respectively the equation (5.26), the following matrix elements must be replaced corresponding to the models derived in chapter 3:

$\boldsymbol{\Phi}$ by $\boldsymbol{\Phi}_{11}^f$, $\mathbf{H}$ by $\mathbf{H}_1^f$ and $\mathbf{h}$ by $\boldsymbol{\Phi}_{12}^f$

From equation (3.54) it will be obtained:

$$\boldsymbol{\Phi}_{11}^f = \begin{bmatrix} \boldsymbol{\Phi}_{11} & \boldsymbol{\Phi}_{12} \\ -\boldsymbol{\Phi}_{12} & \boldsymbol{\Phi}_{11} \end{bmatrix} = \begin{bmatrix} 1 - \dfrac{T}{\sigma}\left(\dfrac{1}{T_s} + \dfrac{1-\sigma}{T_r}\right) & \omega_s T \\ -\omega_s T & 1 - \dfrac{T}{\sigma}\left(\dfrac{1}{T_s} + \dfrac{1-\sigma}{T_r}\right) \end{bmatrix} \tag{5.27}$$

$$\mathbf{\Phi}_{12}^{f} = \begin{bmatrix} \Phi_{13} & \Phi_{14} \\ -\Phi_{14} & \Phi_{13} \end{bmatrix} = \begin{bmatrix} \dfrac{1-\sigma}{\sigma}\dfrac{T}{T_r} & \dfrac{1-\sigma}{\sigma}\omega T \\ -\dfrac{1-\sigma}{\sigma}\omega T & \dfrac{1-\sigma}{\sigma}\dfrac{T}{T_r} \end{bmatrix} \tag{5.28}$$

$$\mathbf{H}_{1}^{f} = \begin{bmatrix} h_{11} & 0 \\ 0 & h_{11} \end{bmatrix} = \begin{bmatrix} \dfrac{T}{\sigma L_s} & 0 \\ 0 & \dfrac{T}{\sigma L_s} \end{bmatrix} \tag{5.29}$$

If the matrix elements from (5.27), (5.28) and (5.29) are used in the equation (5.26) now, the following controller equations will be obtained considering that the cross component ψ_{rq} of the rotor flux is zero because of an exact field orientation:

$$\begin{cases} u_{sd}(k+1) = h_{11}^{-1}\left[x_{wd}(k) - \Phi_{11}\,x_{wd}(k-1) - \Phi_{12}\,x_{wq}(k-1) \right. \\ \qquad\qquad \left. + y_d(k-2) - \Phi_{13}\,\psi_{rd}^{/}(k+1)\right] \\ u_{sq}(k+1) = h_{11}^{-1}\left[x_{wq}(k) + \Phi_{12}\,x_{wd}(k-1) - \Phi_{11}\,x_{wq}(k-1) \right. \\ \qquad\qquad \left. + y_q(k-2) + \Phi_{14}\,\psi_{rd}^{/}(k+1)\right] \end{cases} \tag{5.30}$$

Because of the necessary storage of the temporary variable **y** through several sampling periods a direct programming of the equation (5.30) is impractical. The following sequence is more advantageous:

1. Calculation of the vector **y**(k) using (5.25):

$$\begin{cases} y_d(k) = x_{wd}(k) - \Phi_{11}\,x_{wd}(k-1) - \Phi_{12}\,x_{wq}(k-1) + y_d(k-2) \\ y_q(k) = x_{wq}(k) + \Phi_{12}\,x_{wd}(k-1) - \Phi_{11}\,x_{wq}(k-1) + y_q(k-2) \end{cases} \tag{5.31}$$

2. Then calculation of the stator voltage using (5.17):

$$\begin{cases} u_{sd}(k+1) = h_{11}^{-1}\left[y_d(k) - \Phi_{13}\,\psi_{rd}^{/}(k+1)\right] \\ u_{sq}(k+1) = h_{11}^{-1}\left[y_q(k) + \Phi_{14}\,\psi_{rd}^{/}(k+1)\right] \end{cases} \tag{5.32}$$

Now the equations (5.31) and (5.32) can be used for programming provided that the axis-related deviations x_{wd}, x_{wq}, and the accumulated quantity **y** still must be corrected at stator voltage limitation to avoid instabilities. The subchapter 5.5 will deal with the problem of the control variable limitation later in detail.

b) Use of the controller for the IM in stator-fixed coordinates

$\boldsymbol{\Phi}$, **H** and **h** are replaced by $\boldsymbol{\Phi}_{11}^{s}$, $\mathbf{H}_{1}^{s}$ and $\boldsymbol{\Phi}_{12}^{s}$ from the equation (3.50):

$$\boldsymbol{\Phi}_{11}^{s}=\begin{bmatrix}\Phi_{11} & 0\\ 0 & \Phi_{11}\end{bmatrix}=\begin{bmatrix}1-\dfrac{T}{\sigma}\left(\dfrac{1}{T_s}+\dfrac{1-\sigma}{T_r}\right) & 0\\ 0 & 1-\dfrac{T}{\sigma}\left(\dfrac{1}{T_s}+\dfrac{1-\sigma}{T_r}\right)\end{bmatrix} \tag{5.33}$$

$$\boldsymbol{\Phi}_{12}^{s}=\begin{bmatrix}\Phi_{13} & \Phi_{14}\\ -\Phi_{14} & \Phi_{13}\end{bmatrix}=\begin{bmatrix}\dfrac{1-\sigma}{\sigma}\dfrac{T}{T_r} & \dfrac{1-\sigma}{\sigma}\omega T\\ -\dfrac{1-\sigma}{\sigma}\omega T & \dfrac{1-\sigma}{\sigma}\dfrac{T}{T_r}\end{bmatrix} \tag{5.34}$$

$$\mathbf{H}_{1}^{s}=\begin{bmatrix}h_{11} & 0\\ 0 & h_{11}\end{bmatrix}=\begin{bmatrix}\dfrac{T}{\sigma L_s} & 0\\ 0 & \dfrac{T}{\sigma L_s}\end{bmatrix} \tag{5.35}$$

If the matrix elements of (5.33), (5.34) and (5.35) are inserted into the equation (5.26), then the following voltage components in $\alpha\beta$ coordinates will be obtained.

$$\begin{cases} u_{s\alpha}(k+1)=h_{11}^{-1}\left[x_{w\alpha}(k)-\Phi_{11}\,x_{w\alpha}(k-1)+y_{\alpha}(k-2)\right.\\ \qquad\qquad \left.-\Phi_{13}\,\psi'_{r\alpha}(k+1)-\Phi_{14}\,\psi'_{r\beta}(k+1)\right]\\ u_{s\beta}(k+1)=h_{11}^{-1}\left[x_{w\beta}(k)-\Phi_{11}\,x_{w\beta}(k-1)+y_{\beta}(k-2)\right.\\ \qquad\qquad \left.+\Phi_{14}\,\psi'_{r\alpha}(k+1)-\Phi_{13}\,\psi'_{r\beta}(k+1)\right] \end{cases} \tag{5.36}$$

The next steps are again useful to support programming:

1. Calculation of the vector **y**(k) according to (5.25):

$$\begin{cases} y_{\alpha}(k)=x_{w\alpha}(k)-\Phi_{11}\,x_{w\alpha}(k-1)+y_{\alpha}(k-2)\\ y_{\beta}(k)=x_{w\beta}(k)-\Phi_{11}\,x_{w\beta}(k-1)+y_{\beta}(k-2) \end{cases} \tag{5.37}$$

2. Then the calculation of the voltage using (5.17):

$$\begin{cases} u_{s\alpha}(k+1)=h_{11}^{-1}\left[y_{\alpha}(k)-\Phi_{13}\,\psi'_{r\alpha}(k+1)-\Phi_{14}\,\psi'_{r\beta}(k+1)\right]\\ u_{s\beta}(k+1)=h_{11}^{-1}\left[y_{\beta}(k)+\Phi_{14}\,\psi'_{r\alpha}(k+1)-\Phi_{13}\,\psi'_{r\beta}(k+1)\right] \end{cases} \tag{5.38}$$

c) Use of the controller for the PMSM in field synchronous coordinates

Instead of $\mathbf{\Phi}$, $\mathbf{H}$ and $\mathbf{h}$, the matrices $\mathbf{\Phi}_{SM}^{f}$, $\mathbf{H}_{SM}^{f}$ and $\mathbf{h}$ from equations (3.71) and (3.72) are used for the PMSM:

$$\mathbf{\Phi}_{SM}^{f} = \begin{bmatrix} \Phi_{11} & \Phi_{12} \\ \Phi_{21} & \Phi_{22} \end{bmatrix} = \begin{bmatrix} 1 - \dfrac{T}{T_{sd}} & \omega_s T \dfrac{L_{sq}}{L_{sd}} \\ -\omega_s T \dfrac{L_{sd}}{L_{sq}} & 1 - \dfrac{T}{T_{sq}} \end{bmatrix} \tag{5.39}$$

$$\mathbf{H}_{SM}^{f} = \begin{bmatrix} h_{11} & 0 \\ 0 & h_{22} \end{bmatrix} = \begin{bmatrix} \dfrac{T}{L_{sd}} & 0 \\ 0 & \dfrac{T}{L_{sq}} \end{bmatrix}; \quad \mathbf{h} = \begin{bmatrix} 0 \\ -\dfrac{\omega_s T}{L_{sq}} \end{bmatrix} = \begin{bmatrix} 0 \\ h_2 \end{bmatrix} \tag{5.40}$$

After replacing the matrix elements of (5.39), (5.40), the *dq* components of the stator voltage result to:

$$\begin{cases} u_{sd}(k+1) = h_{11}^{-1}\left[x_{wd}(k) - \Phi_{11}\, x_{wd}(k-1) - \Phi_{12}\, x_{wq}(k-1) + y_d(k-2)\right] \\ u_{sq}(k+1) = h_{22}^{-1}\left[x_{wq}(k) - \Phi_{21}\, x_{wd}(k-1) - \Phi_{22}\, x_{wq}(k-1) + y_q(k-2) - h_2\, \psi_p\right] \end{cases} \tag{5.41}$$

and the following programming equations will be obtained:

1. **y**(k) is calculated by using (5.25):

$$\begin{cases} y_d(k) = x_{wd}(k) - \Phi_{11}\, x_{wd}(k-1) - \Phi_{12}\, x_{wq}(k-1) + y_d(k-2) \\ y_q(k) = x_{wq}(k) - \Phi_{21}\, x_{wd}(k-1) - \Phi_{22}\, x_{wq}(k-1) + y_q(k-2) \end{cases} \tag{5.42}$$

2. then the voltage calculation using (5.17) follows:

$$\begin{cases} u_{sd}(k+1) = h_{11}^{-1}\, y_d(k) \\ u_{sq}(k+1) = h_{22}^{-1}\left[y_q(k) - h_2\, \psi_p\right] \end{cases} \tag{5.43}$$

5.3.2 Design of a current vector controller with dead-beat behaviour for integrating measurement of the current actual-values

In principle the process equations (5.18) and (5.19) are only valid for processes with instantaneous value measurement of the current values. In case of an integrating measurement (cf. subchapter 4.1) the measuring equipment is modeled by using the averaging function:

$$\mathbf{i}_s^M(k) = \frac{1}{2}\left[\mathbf{i}_s(k) + \mathbf{i}_s(k-1)\right] \tag{5.44}$$

raised index M: average value

and the result $\mathbf{i}_s^M(k)$ is available for the control as actual value of the stator current. The final process equation in case of integrating measurement results from (5.44) by using (5.18):

$$\mathbf{i}_s^M(k+1) = \mathbf{\Phi}\,\mathbf{i}_s^M(k) + \frac{1}{2}\left[\mathbf{y}(k-1) + \mathbf{y}(k-2)\right] \tag{5.45}$$

and in the z domain:

$$\left[z\mathbf{I} - \mathbf{\Phi}\right]\mathbf{i}_s^M(z) = \frac{1}{2}\left[z^{-1} + z^{-2}\right]\mathbf{y}(z) \tag{5.46}$$

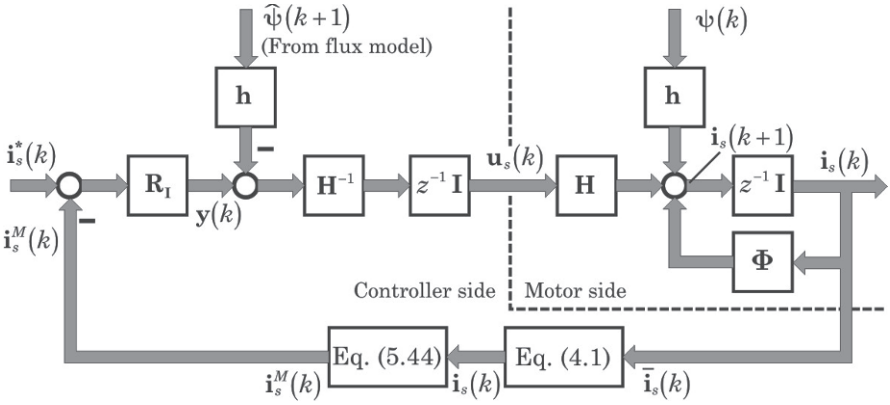

Fig. 5.16 Block structure of the current vector controller for IM or PMSM with integrating measurement

The controller equation starts from:

$$\mathbf{y}(z) = \mathbf{R_I}\left[\mathbf{i}_s^*(z) - \mathbf{i}_s^M(z)\right] \tag{5.47}$$

After eliminating **y**(z) in (5.46) and (5.47) we obtain the transfer function:

$$\mathbf{i}_s^M(z) = \frac{1}{2}\left(z^{-1} + z^{-2}\right)\left[z\mathbf{I} - \mathbf{\Phi} + \frac{1}{2}\left(z^{-1} + z^{-2}\right)\mathbf{R_I}\right]^{-1}\mathbf{R_I}\,\mathbf{i}_s^*(z) \tag{5.48}$$

The approach for the closed loop response and respectively the reference transfer function is:

$$\mathbf{i}_s^M(z) = \frac{1}{2}\left(z^{-2} + z^{-3}\right)\mathbf{i}_s^*(z) \tag{5.49}$$

This is equivalent to a dead beat response. The equations (5.48) and (5.49) are identical, if the following controller is chosen:

$$\mathbf{R_I} = \frac{\mathbf{I} - z^{-1}\mathbf{\Phi}}{1 - \frac{1}{2}\left(z^{-2} + z^{-3}\right)} \tag{5.50}$$

The equation (5.50) looks as follows in the time domain:

$$\begin{aligned} \mathbf{y}(k) &= \mathbf{x}_w(k) - \mathbf{\Phi}\,\mathbf{x}_w(k-1) + \frac{1}{2}\left[\mathbf{y}(k-2) + \mathbf{y}(k-3)\right] \\ \mathbf{x}_w(k) &= \mathbf{i}_s^*(k) - \mathbf{i}_s^M(k) \end{aligned} \tag{5.51}$$

The derivation of the equations for the controller application in figure 5.16 can similarly be carried out – for the cases IM or PMSM, in field synchronous or stator fixed coordinates – like in the subchapter 5.3.1. For the problem of the control variable limitation it is again referred to the subchapter 5.5.

5.3.3 Design of a current vector controller with finite adjustment time

The controllers introduced in this chapter are derived like in chapter 5.3.1 from the common theoretical approach (5.11) for the closed loop response.

It was shown repeatedly in the literature references mentioned at the beginning of the subchapter 5.3 that the fastest dynamics can be achieved by a dead beat design. This approach provides a virtually undelayed torque impression which is particularly advantageous for the conception of superimposed control loops for mechanical systems (speed, position). Step response times of under 1 ms were reached. The application of fast microprocessors (digital signal processors, high performance microcontrollers) and the tendency toward higher pulse frequencies (10-kHz and more) however result in yet faster sampling of the current control (T = 100...200 µs). If the current control was prepared for dead beat behaviour, the inverter could not produce the voltage over time areas necessary to drive the required current step amplitudes (at dynamic processes like magnetization, start up or speed reversal) within the very short demanded rise times of 2×100µs ... 2×200µs = 200...400µs. This is extremely critical for inverters with small control reserve (low DC link voltage). It becomes critical as well if the drive is operated at the voltage limit and dynamic processes (e.g. speed reversal out of the field weakening range) take place simultaneously. Preferably, at these small sampling times and with fast processors like DSP's the current control is not adjusted to

dead beat response any more, but to FAT behaviour with more than 2 steps response time. As indicated in the section 5.2 it would be realistic to realize the FAT behaviour with 3 or 4 sampling steps.

For instantaneous value measuring of the stator currents the transfer function (5.21) results for the current-controlled IM in *dq* coordinates. The reference transfer functions for the recommended step number are given in (5.13) and (5.14). The equation (5.21) is identical with either (5.13) or (5.14), if for:

1. **n=2** (FAT = *n*+1 = 3) the following controller:

$$\mathbf{R_I} = \frac{1}{2}\frac{\left(1+z^{-1}\right)\left[\mathbf{I}-z^{-1}\mathbf{\Phi}\right]}{1-\frac{1}{2}\left(z^{-2}+z^{-3}\right)}, \text{ and} \tag{5.52}$$

2. **n=3** (FAT = *n*+1 = 4) the following controller:

$$\mathbf{R_I} = \frac{1}{3}\frac{\left(1+z^{-1}+z^{-2}\right)\left[\mathbf{I}-z^{-1}\mathbf{\Phi}\right]}{1-\frac{1}{3}\left(z^{-2}+z^{-3}+z^{-4}\right)} \tag{5.53}$$

is valid. The controller designs (5.52) and (5.53) can be used – regarding the available processing capacity – almost without problems by application of digital signal processors with a sampling period of 100 µs, including necessary functions like the vector modulation, the coordinate transformation, the flux model or flux observer and the feedback value processing. The outlined design was carried out assuming an instantaneous value measurement of the stator current.

The current driving voltage over time area is – in comparison with the dead beat design – the same, but distributed over several steps. With that the control voltage $\mathbf{u}_s$ rarely goes into the limitation. This property is seen as an important advantage, especially for inverters with small control reserve (low DC voltage). This also takes effect particularly if the inverter is operated at the limits of the control reserve (e.g. in the field weakening area or at full load). The system stability is fundamentally improved while entering into and recovering from limitation.

5.4 Design of a current state space controller with dead beat behaviour

The main advantage of the *current vector regulators* introduced in the chapters 5.3.1 and 5.3.3 is primarily the practically proven ruggedness when applied to machines whose data are known only inaccurately or calculated only from the name plate. This chapter on the other hand introduces a design in the state space which can produce superior qualities with respect to smooth running and dynamical or decoupling behaviour at higher stator frequencies if exact machine data are available. This allows the particularly advantageous use of the new controller, called *the current state controller* from now on (figure 5.17), in precision drives.

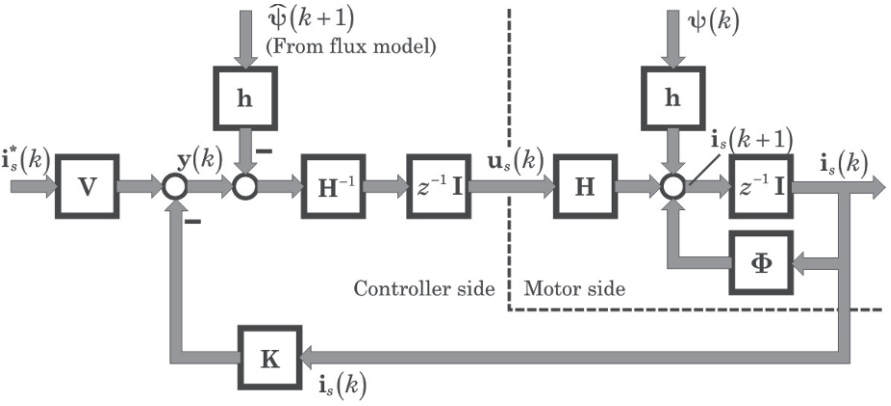

Fig. 5.17 Block structure of the current state controller with pre-filter matrix **V** and feedback matrix **K**

The design starts out as usual from the general approach (5.17) and from the compensated process model (5.18) or (5.19). The controller equation can be written in the *z* domain as:

$$\mathbf{y}(z) = \mathbf{V}\,\mathbf{i}_s^*(z) - \mathbf{K}\,\mathbf{i}_s(z) \tag{5.54}$$

The equation of the closed loop system is obtained after inserting the equation (5.54) into (5.19):

$$\left[z\mathbf{I} - \left(\mathbf{\Phi} - z^{-1}\mathbf{K}\right)\right]\mathbf{i}_s(z) = z^{-1}\mathbf{V}\,\mathbf{i}_s^*(z) \tag{5.55}$$

Using equation (5.55), the state controller can be designed now, and it has to be noticed that

1. the *feedback matrix* **K** changes the pole positions of the closed loop system, and is therefore decisive for *dynamics* and *stability*. With that, different design strategies, such as the design

- on dead beat behaviour or
- on well damped characteristic, can be derived, and

2. the *pre-filter matrix* **V** serves the adjustment of the demanded working point, and therefore is responsible for the *stationary transfer characteristic*.

This means with respect to the decoupling between the torque and flux forming current components that **K** determines *the dynamic* and **V** *the static decoupling properties*.

5.4.1 Feedback matrix K

By using (5.55) the characteristic equation of the closed loop system is:

$$\det\left[z\,\mathbf{I}-\left(\mathbf{\Phi}-z^{-1}\mathbf{K}\right)\right]=0 \tag{5.56}$$

The polynomial on the left side of (5.56) has the following general form:

$$\det\left[z\,\mathbf{I}-\left(\mathbf{\Phi}-z^{-1}\mathbf{K}\right)\right]=\sum_{i=0}^{\infty}a_i\,z^i \tag{5.57}$$

The system has two poles. To achieve dead beat behaviour, both poles must be located (see e.g. Föllinger [1982]) in the coordinate origin. This means that

$$a_i=0 \;\text{ for }\; i\neq 2\,;\; a_2=1$$

Following the Cayley-Hamilton theorem (cf. Föllinger [1982], Isermann [1987]) the matrix $(\mathbf{\Phi}-z^{-1}\mathbf{K})$ fulfils its own characteristic equation. From that, we obtain:

$$\left[\mathbf{\Phi}-z^{-1}\mathbf{K}\right]^2=\mathbf{0} \;\text{ or }\; \left[\mathbf{\Phi}-z^{-1}\mathbf{K}\right]=\mathbf{0} \tag{5.58}$$

and then:

$$\mathbf{K}=z\,\mathbf{\Phi} \tag{5.59}$$

Two remarks shall follow to interpret this result:

1. The equation (5.59) contains a z operator, which means that a *prediction* (one sampling period in advance) of the actual-value of the stator current is necessary.
2. The dead beat behaviour would cause large control amplitudes (as explained in the subchapter 5.3.3) at set point steps, and from this, strong control movements for stochastically disturbed control variables. Therefore the design (5.59) could have an unfavourable effect for inverters with small control reserve (low DC link voltage). A FAT behaviour according to the subchapter 5.3.3 would be sensible

and useful. The application of this reference transfer function in the state space, however, is not possible. A behaviour prepared for a good damping is, on the other hand, practicable. The poles then should not be assigned directly in the coordinate origin but in its near vicinity.

$$\det\left[z\mathbf{I}-\left(\mathbf{\Phi}-z^{-1}\mathbf{K}\right)\right]=\left(z-z_1\right)^2 \quad \text{with } z_1\neq 0 \tag{5.60}$$

From (5.60) it will be obtained:

$$\mathbf{K}=z\left[\mathbf{\Phi}-z_1\mathbf{I}\right] \tag{5.61}$$

For practical realization it suffices to determine the satisfactory behaviour by varying z_1 experimentally without having to exaggerate the theory here further.

5.4.2 Pre-filter matrix V

A stationary exact transfer characteristic and good decoupling between the two current components can be expected if the following is valid:

$$\mathbf{i}_s\left(k+1\right)=\mathbf{i}_s\left(k\right)=\mathbf{i}_s^*\left(k\right) \quad \text{für } k\to\infty$$

or:

$$\mathbf{i}_s\left(z\right)=\mathbf{i}_s^*\left(z\right) \quad \text{für } z\to 1$$

It follows from (5.55):

$$\mathbf{V}=\mathbf{I}-\left[\mathbf{\Phi}-\mathbf{K}\right] \tag{5.62}$$

After using the matrix $\mathbf{K}$ like (5.59) or (5.61) it will be obtained:

1. For the dead beat behaviour:

$$\mathbf{V}=\mathbf{I} \tag{5.63}$$

2. For the design with good damping:

$$\mathbf{V}=\left(1-z_1\right)\mathbf{I} \tag{5.64}$$

With $\mathbf{K}$ and $\mathbf{V}$ calculated by equations (5.59) and (5.63) or (5.61) and (5.64) we obtain from (5.55) the following transfer function of the controlled process:

1. For the dead beat behaviour:

$$\mathbf{i}_s\left(z\right)=z^{-2}\,\mathbf{i}_s^*\left(z\right) \tag{5.65}$$

2. For the design with good damping:

$$\mathbf{i}_s\left(z\right)=\frac{1-z_1}{1-z_1 z}\mathbf{i}_s^*\left(z\right) \tag{5.66}$$

The two state space designs point to a good dynamic decoupling judging from their diagonal transfer matrices. In contrast to the current vector controller (cf. subchapter 5.3) however, a stationary error has always to be

expected because of *the missing integral term*. This stationary error, partly caused by the first order approximation of the discrete state models and partly caused by parameter deviations, shall be eliminated by introducing an additional integral term. Because the current components are dynamically and statically decoupled by the controller design with **K** and **V**, the elimination of the stationary error or deviation can be realized separately for every single current component. Therefore the control structure is extended by two additional integral controllers (figure 5.18).

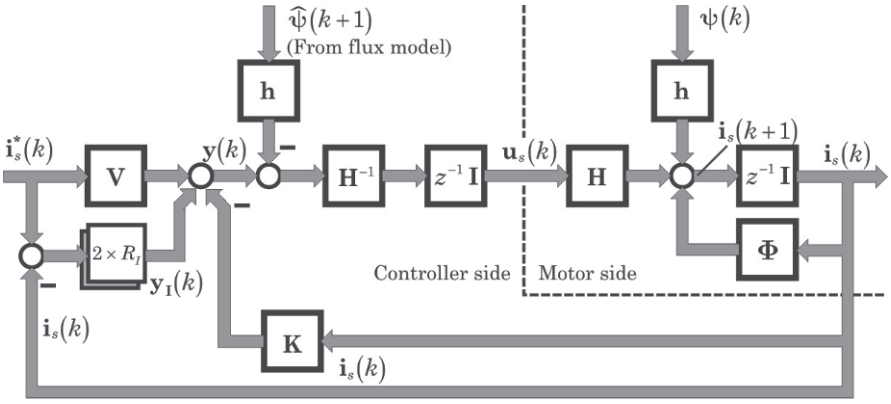

Fig. 5.18 Current state space control with two additional integral controllers

The equation of the additional integral controller R_I will be:

$$\left(1-z^{-1}\right)\mathbf{y_I}(z)=V_I\,\Delta\mathbf{i}_s(z) \quad \text{or}$$
$$\mathbf{y_I}(k)=V_I\,\Delta\mathbf{i}_s(k)+\mathbf{y_I}(k-1) \tag{5.67}$$

V_I Controller gain
$\Delta\mathbf{i}_s$ Stationary current error
$\mathbf{y_I}$ Output variable of the integral controller

The controller output variables $\mathbf{y}_\mathrm{I}$ have the task to eliminate the stationary errors $\Delta\mathbf{i}_s$ of the stator current. $\mathbf{y}_\mathrm{I}$ and $\Delta\mathbf{i}_s$ also fulfill the process equations (5.18) and (5.19):

$$\left[z\mathbf{I}-\mathbf{\Phi}\right]\Delta\mathbf{i}_s(z)=z^{-1}\mathbf{y_I}(z) \quad \text{or}$$
$$\Delta\mathbf{i}_s(k+1)=\mathbf{\Phi}\,\Delta\mathbf{i}_s(k)+\mathbf{y_I}(k-1) \tag{5.68}$$

Since an effective decoupling between the current components is already ensured by the basic structure of the current state space control, the equations (5.67) and (5.68) can be re-written in component notation as follows:

$$\text{Controller}: \quad y_{Id,q}(z) = \frac{V_{Id,q}}{1 - z^{-1}} \Delta i_{sd,q}(z)$$
$$\text{Process}: \quad \Delta i_{sd,q}(z) = \frac{z^{-2}}{1 - \Phi_{11} z^{-1}} y_{Id,q}(z) \qquad [1] \tag{5.69}$$

The equation (5.69) is substituted into the closed loop transfer function to calculate the gain factors $V_{Id,q}$ which are usually chosen identical. Because these factors correspond to the ratio T/T_I, (T_I is in comparison with the sampling time T a very big integration time), it suffices in the practice to choose for these factors after the normalizing (about normalizing: subchapter 12.1) a value of approx. 0.05 … 0.25.

An even better choice would be to feed the integral controller with the current feedback not directly but through a model of the closed loop control system. This would prevent the controller from being invoked at every set point change.

The reader's attention was already drawn to the z operator in equations (5.59), (5.61). The z operator requires a prediction of the stator current. With the actually realized stator voltage, the estimated rotor flux and the measured stator current this prediction can be simply carried out according to the equation (3.74).

$$\hat{\mathbf{i}}_s(k+1) = \mathbf{\Phi}\,\mathbf{i}_s(k) + \mathbf{H}\,\mathbf{u}_s(k) + \mathbf{h}\,\hat{\psi}(k) \tag{5.70}$$

The equation (5.70) has to be adapted to the usage of IM or PMSM and in which coordinate system the motor will be controlled. The complete structure of the current state space control is represented in the figure 5.19.

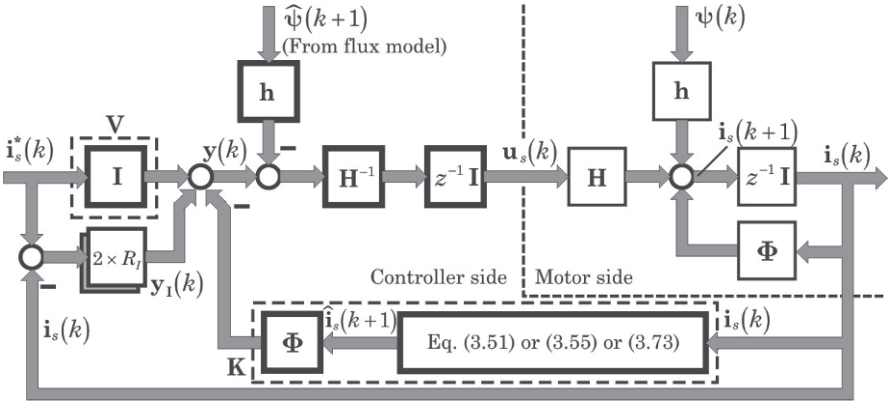

Fig. 5.19 Detailed block structure of the current state space controller for the IM and PMSM

[1] Caution: Instead of $\mathbf{\Phi}_{11}$, $\mathbf{\Phi}_{22}$ is used for q axis in the case PMSM

5.5 Treatment of the limitation of control variables

Generally, the control variable or the stator voltage is limited by the DC link voltage. At uncertain time, e.g. because of a dynamic transient, the current controller requires excessive amplitudes of the control variable which, however, cannot be provided by the inverter. So the control variable hits its maximum consuming all available control reserve. After the current has reached its reference the control variable still stays on its maximum until the integral part has decayed. In this process, oscillations or vibrations of the controlled variable around limitation may develop.

The described process is known and understandable. It is also known that these difficulties can be normally solved by *switching off the integral part* (*anti-reset windup*) once the control variable goes into the limitation. Regarding the new current controllers this strategy could be applied for the additional integral parts of the current state space controller because these parts do obviously exist separately. What would, however, happen with the current vector controllers? The integral part is here not recognizable as part of the design in its own right. Furthermore, being a rather empirical method, turning-off the integrating part does not fit into a fully consistent design and leaves a number of open questions as to the optimal instants to disable and re-enable integration. A better and consistent solution can be provided by reverse-correction of the control deviation (cf. Schönfeld [1985]) which is elaborated on further in this chapter.

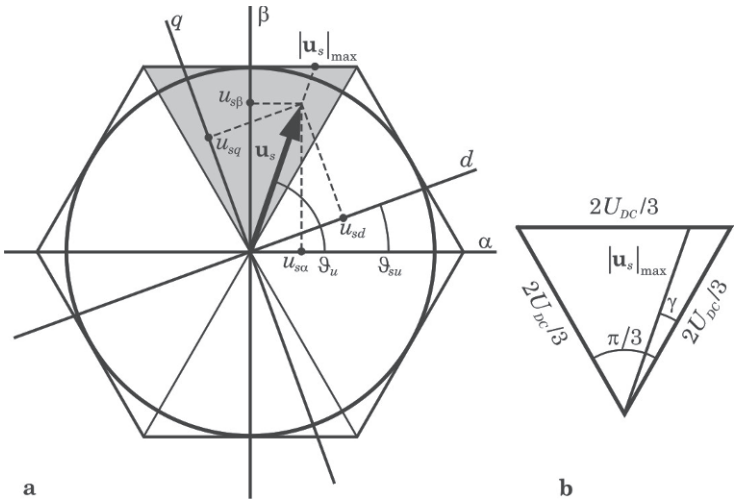

Fig. 5.20 Limitation of control variable: (**a**) Voltage vector $\mathbf{u}_s$ with arbitrary phase angle ϑ_u and (**b**) the maximum modulation ratio $|\mathbf{u}_s|_{max}$ of inverter

Instead of measuring the stator voltage to detect when entering limitation, the stator voltage can be limited intentionally to the maximum modulation ratio.

From the chapter 2 is known, that the maximum usable stator voltage lies within a hexagon (fig. 5.20) and furthermore, that only the limitation of the amplitude of the voltage vector is of importance. However, the stator voltage actually exists in components, u_{sd} and u_{sq} or $u_{s\alpha}$ und $u_{s\beta}$. That means:

> *The voltage limitation must be split into components as well. Suitable methods for this have to be worked out for the chosen coordinate system.*

The voltage limitation itself is completed with its splitting into components. But as mentioned above:

> *A reverse correction strategy, which prevents the vibrations or oscillations caused by the implicitly existing integral part, must be worked out.*

The figure 5.20a has pointed to the possibilities of setting the limitation boundaries on the inner circle touched by the hexagon or on the outer hexagon. The limitation most simply works with the circle, but a loss of control reserve (the area between hexagon and circle) would be the result. The phase angle ϑ_u of the stator voltage then is:

$$\vartheta_u = \vartheta_{su} + \arctan\left(\frac{u_{sq}}{u_{sd}}\right) \tag{5.71}$$

With the help of (5.71) and fig. 5.20b the maximum amplitude of the voltage vector or the maximum modulation ratio (at normalization with $2U_{DC}/3$) depending on the phase angle can be found as:

$$\left|\mathbf{u_s}\right|_{\max} = \frac{\sqrt{3}}{2}\frac{1}{\sin\left(\gamma + \frac{\pi}{3}\right)}^{1} \tag{5.72}$$

The limitation on the outer hexagon according to (5.72) yields the best actuator utilization with respect to deliverable control voltage, however, causes an additional third harmonic in the current. This is unwanted in the stationary operation where the field and torque forming components represent DC quantities. It is therefore recommended for high-quality servo drives to limit on the inner circle. The maximum modulation ratio then is:

---

[1] After normalizing with $2U_{DC}/3$ the voltage is formulated as modulation ratio here; the angle γ is defined in fig. 5.20b.

$$\left|\mathbf{u_s}\right|_{\max} = \frac{\sqrt{3}}{2} \tag{5.73}$$

In principle the limitation can be implemented on one of the three following levels (fig. 5.21).

1. *Level of dq components:* This is the mostly applied, most effective variant for the limitation. The decoupling between the *dq* axes or between torque formation and magnetization can be ensured largely with a correct splitting strategy (cf. chapter 5.5.1).
2. *Level of αβ components:* The application of this variant is only possible if the torque impression is implemented using a current controller in the stator-fixed coordinate system. Unfortunately, the decoupling between torque formation and magnetization cannot be ensured any more.
3. *Level of switching times:* This variant is rarely used. The decoupling is not ensured any more. For low-quality drives, where microprocessor power (for splitting and reverse correction) is missing and/or slow semiconductor components are used, the use of this variant could be interesting.

The following chapters only deal with the limitation at the level of the *dq* coordinate system.

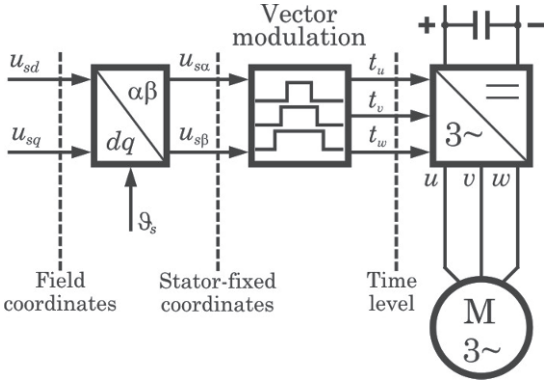

Fig. 5.21 Possible levels for the realization of the control variable limitation

5.5.1 Splitting strategy at voltage limitation

Geometrically the voltage limitation is equivalent to shortening the voltage amplitude. For non-reactive loads, i.e. current and voltage have the same sign, the current gets smaller at reduced voltage. For reactive,

inductive/capacitive or mixed (ohmic-inductive, ohmic-capacitive) loads – i.e. current and voltage can have different signs – a voltage shortening would be able to cause the current to increase and duly cause the system to become instable. It is known that u_{sd} and i_{sd} as well as u_{sq} and i_{sq} very often have different signs which indicate the operating state (motor, generator) of the system.

These introductory words make already clear *that a splitting strategy, which ensures the system stability, must be able to recognize priorities for the coordinate axes depending on the operating state and then perform the limit splitting according to the geometric possibilities*.

a) Geometric possibilities for limitation

From geometrical point of view and depending on whether the outer hexagon or the inner circle is chosen as the limitation curve, one of the three following possibilities (cf. figure 5.22) can be used for the splitting:

1. u_{sd} is cut down, u_{sq} will be kept or has priority:

$$u_{sdr} = sign\left(u_{sd}\right)\sqrt{\left|\mathbf{u_s}\right|^2_{\max} - u^2_{sq}} \;;\; u_{sqr} = u_{sq} \tag{5.74}$$

2. u_{sd} and u_{sq} are truncated in the same proportion (called: the phase correct limitation):

$$u_{sdr} = u_{sd}\sqrt{\frac{\left|\mathbf{u_s}\right|^2_{\max}}{u^2_{sd} + u^2_{sq}}} \;;\; u_{sqr} = u_{sq}\sqrt{\frac{\left|\mathbf{u_s}\right|^2_{\max}}{u^2_{sd} + u^2_{sq}}} \tag{5.75}$$

3. u_{sq} is cut down, u_{sd} will be kept or has priority:

$$u_{sdr} = u_{sd} \;;\; u_{sqr} = sign\left(u_{sq}\right)\sqrt{\left|\mathbf{u_s}\right|^2_{\max} - u^2_{sd}} \tag{5.76}$$

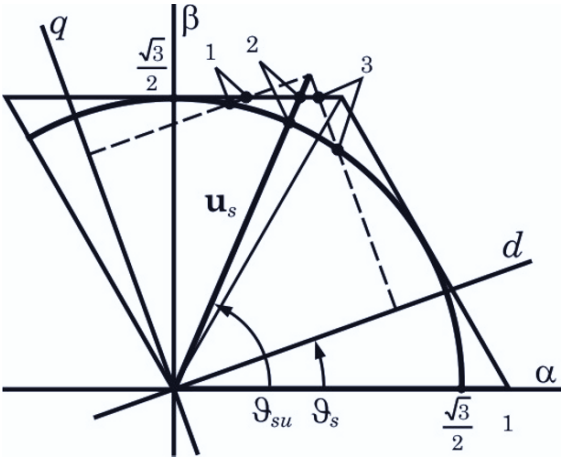

Fig. 5.22 Geometric possibilities for limitation splitting: (**1**) only *d* component, or (**2**) *d* and *q* component in the same proportion, or (**3**) only *q* component will be truncated

The figure 5.22 clarifies that with the inner circle as limitation curve the value of the maximum modulation ratio $|\mathbf{u}_s|_{\max}$ is always given according to (5.73). Unlike this, $|\mathbf{u}_s|_{\max}$ using the outer hexagon can adopt different values (cf. fig. 5.22) for the same reference voltage vector, whose complex calculation cannot be handled by every microprocessor and therefore is rarely used. For this reason the limitation on the hexagon will not be further followed here.

The equations (5.74) and (5.76) point to the possible case in which even the component with priority can exceed the value of $|\mathbf{u}_s|_{\max}$. In this case the component with priority must also be shortened.

b) Splitting strategy by [Quang 1994]

The strategy starts out from an analysis of the possible operating states of the electrical machine.

Asynchronous drive using IM

In stationary operation the following system of equations is valid for the stator voltage:

$$\begin{cases} u_{sd} = R_s\, i_{sd} - \omega_s\, \sigma\, L_s\, i_{sq} \\ u_{sq} = R_s\, i_{sq} + \omega_s\, L_s\, i_{sd} \end{cases} \tag{5.77}$$

The operating states which lead to the voltage limitation are always connected to higher frequencies so that resistive voltage drops are negligible in the equation (5.77). Therefore they can be reduced to:

$$\begin{cases} u_{sd} \approx -\omega_s\, \sigma\, L_s\, i_{sq} \\ u_{sq} \approx \omega_s\, L_s\, i_{sd} \end{cases} \tag{5.78}$$

The equation (5.78) obviously points to a static coupling between *d* and *q* axes and implies that in the area of higher frequencies (where limitations often take place) the components u_{sd} and u_{sq} usually have to provide the greater part for overcoming this coupling than for keeping its own current component. The following facts can be stated in evaluation of equation (5.78):

- The field forming current i_{sd} *always has positive sign in stationary operation.* (Remark: The field forming current i_{sd} could accept negative sign only for feedback-controlled flux for a short time).
- *The product* $m_M \times \omega_s$ *or* $i_{sq} \times \omega_s$ *is always positive in motor operation*. I.e. i_{sq} and ω_s always have the same sign. This means, that:
  $\Rightarrow u_{sd} < 0$, or u_{sd} and i_{sd} have different signs, and
  $\Rightarrow u_{sq}$ and i_{sq} have the same sign.

- *The product $m_M \times \omega_s$ or $i_{sq} \times \omega_s$ is always negative in generator operation.* I.e. i_{sq} and ω_s always have different signs. This means, that:
  $\Rightarrow u_{sd} > 0$, or u_{sd} and i_{sd} have *the same sign*, and
  $\Rightarrow u_{sq}$ and i_{sq} have *different signs*.
  The above short analysis says, that:
- In motor operation the component u_{sd} and
- in generator operation the component u_{sq}

will get priority. If the priority component already exceeds the value $|\mathbf{u}_s|_{\max}$, so approx. 95% of $|\mathbf{u}_s|_{\max}$ shall be assigned to this component.

Synchronous drive using PMSM

The following relation will be arrived at for the synchronous drive in stationary operation similar to the case of the asynchronous drive:

$$\begin{cases} u_{sd} = R_s\, i_{sd} - \omega_s\, L_{sq}\, i_{sq} \\ u_{sq} = R_s\, i_{sq} + \omega_s\, L_{sd} \left(i_{sd} + \dfrac{\psi_p}{L_{sd}} \right) \end{cases} \tag{5.79}$$

or

$$\begin{cases} u_{sd} \approx -\omega_s\, L_{sq}\, i_{sq} \\ u_{sq} \approx \omega_s\, L_{sd} \left(i_{sd} + \dfrac{\psi_p}{L_{sd}} \right) \end{cases} \tag{5.80}$$

In the two above equations, the term $\left(i_{sd} + \psi_p / L_{sd}\right)$, in which the current i_{sd} assumes the value zero in the basic operation range and negative values only in the field weakening range, represents the substitute magnetization current with always positive values. The equation (5.80) can be interpreted now similarly to (5.78) of the IM so that the following conclusions can be drawn:

- *The product $m_M \times \omega_s$ or $i_{sq} \times \omega_s$ is always positive in motor operation.* i_{sd} is either zero or negative. This means, that:
  $\Rightarrow u_{sd} < 0$, or u_{sd} and i_{sd} have *the same sign*, and
  $\Rightarrow u_{sq}$ and i_{sq} have *the same sign*.
- *The product $m_M \times \omega_s$ or $i_{sq} \times \omega_s$ is always negative in generator operation.* i_{sd} is either zero or negative. This means, that:
  $\Rightarrow u_{sd} > 0$, or u_{sd} and i_{sd} have *different signs*, and
  $\Rightarrow u_{sq}$ and i_{sq} have *different signs*.

The analysis has shown the clear difference between the IM and the PMSM: While in the motor operation with the IM the component u_{sd} shall

get the priority obviously, the priority must be assigned to none of the axis voltages in the case PMSM.

The generator operation with PMSM seems to be more problematic than with IM because both couples u_{sd}, i_{sd} and u_{sq}, i_{sq} have different signs. Also this case can be realized exactly as for the IM: I.e. priority for u_{sq}. Amplification of $|i_{sd}|$ for a short time after shortening $|u_{sd}|$ only weakens the permanent magnetization which in turn would increase the control reserve, and the limitation would disappear. With these considerations a simple algorithm outlined in figure 5.23 can be worked out for both types of machines.

<table>
<tr><td colspan="4">$|\mathbf{u}_s| > |\mathbf{u}_s|_{\max}$</td></tr>
<tr><td colspan="4">$sign(\omega_s) \neq sign(i_{sq})$?</td></tr>
<tr><td colspan="2">No (motor operation)</td><td colspan="2">Yes (generator operation)</td></tr>
<tr><td colspan="2">$|u_{sd}| > 95\%|\mathbf{u}_s|_{\max}$?</td><td colspan="2">$|u_{sq}| > 95\%|\mathbf{u}_s|_{\max}$?</td></tr>
<tr><td>No</td><td>Yes</td><td>No</td><td>Yes</td></tr>
<tr><td>$u_{sdr} := u_{sd}$
$u_{sqr} := sign(u_{sq}).$
$\sqrt{|\mathbf{u}_s|^2_{\max} - u^2_{sdr}}$</td><td>$u_{sdr} := sign(u_{sd}).$
$(95\%|\mathbf{u}_s|_{\max})$
$u_{sqr} := sign(u_{sq}).$
$\sqrt{|\mathbf{u}_s|^2_{\max} - u^2_{sdr}}$</td><td>$u_{sqr} := u_{sq}$
$u_{sdr} := sign(u_{sd}).$
$\sqrt{|\mathbf{u}_s|^2_{\max} - u^2_{sqr}}$</td><td>$u_{sqr} := sign(u_{sq}).$
$(95\%|\mathbf{u}_s|_{\max})$
$u_{sdr} := sign(u_{sd}).$
$\sqrt{|\mathbf{u}_s|^2_{\max} - u^2_{sqr}}$</td></tr>
</table>

Fig. 5.23 Algorithm for voltage limitation by [Quang 1994] (index *r*: actually realized)

c) Splitting strategy by [Dittrich 1998]

The basic idea of this strategy is ensure decoupling between rotor flux and torque in large-signal behaviour. To achieve this, an intervention in form of a limitation should as much as possible only effect the voltage component, which has caused the maximum voltage vector to exceed its limit, and leave the other component uninfluenced. This concept presumes that such a separation of causes is actually possible and that the voltage vector can be reduced to its maximum value by reduction of one component only. The context is generally more complex and requires a detailed analysis, in particular, if the controlled system must be operated for longer time at the limit of the control variable.

For splitting the voltage limitation after [Dittrich 1998] two questions must be answered:

1. Which component obtains the priority, i.e. which component must remain as unchanged as possible?
2. Which value does the other component get?

The algorithm which is found and realized eventually answers these questions as follows:

Priority decision

Stability considerations are decisive. If current and voltage have different signs in one axis, a limitation of the voltage leads to a temporarily unstable and uncontrollable behavior. If current and voltage signs are different in one axis, this axis must get the priority. If the signs are different in both axes, the axis with the larger current amplitude gets the priority, or the phase correct limitation (using equation (5.75)) is applied. Equal or different signs in the q axis are equivalent to motor or generator operation.

Voltage in the non-priority axis

Two cases have to be distinguished. If the priority component is smaller than the maximum voltage, i.e. the limitation was caused by the non-priority component essentially, the non-priority component results simply from the geometric difference between the maximum voltage and the priority component. In the other case, the non-priority component is assigned the share from the cross-coupling of the current components to support the stationary decoupling of the current components also at control variable limitation.

<table>
<tr><td colspan="4">$|\mathbf{u}_s| > |\mathbf{u}_s|_{\max}$</td></tr>
<tr><td colspan="4">$\left[sign(u_{sd}) \neq sign(i_{sd})\right] \vee \left\{\left[sign(\omega_s) = sign(i_{sq}^*)\right] \wedge \left(i_{sd}^* < 1{,}5\, i_m\right)\right\}$</td></tr>
<tr><td colspan="2">Yes</td><td colspan="2">No</td></tr>
<tr><td colspan="2">$|u_{sd}| > |\mathbf{u}_s|_{\max}$?</td><td colspan="2">$|u_{sq}| > |\mathbf{u}_s|_{\max}$?</td></tr>
<tr><td>Yes</td><td>No</td><td>Yes</td><td>No</td></tr>
<tr><td>$u_{sqr} := \sigma L_s \omega_s i_{sd}$
$u_{sdr} := sign(u_{sd}) \cdot \sqrt{|\mathbf{u}_s|_{\max}^2 - u_{sqr}^2}$</td><td>$u_{sqr} := sign(u_{sq}) \cdot \sqrt{|\mathbf{u}_s|_{\max}^2 - u_{sd}^2}$</td><td>$u_{sdr} := -\sigma L_s \omega_s i_{sq}$
$u_{sqr} := sign(u_{sq}) \cdot \sqrt{|\mathbf{u}_s|_{\max}^2 - u_{sdr}^2}$</td><td>$u_{sdr} := sign(u_{sd}) \cdot \sqrt{|\mathbf{u}_s|_{\max}^2 - u_{sq}^2}$</td></tr>
</table>

Fig. 5.24 Algorithm for voltage limitation by [Dittrich 1998]

The figure 5.24 shows the described algorithm in the overview. A similar approach was attended in [Wiesing 1994].

5.5.2 Correction strategy at voltage limitation

The basic idea of the reverse correction is a correction of the control error $\mathbf{x}_w$ to prevent the windup-integration of the integral part which implicitly exists in the control algorithm.

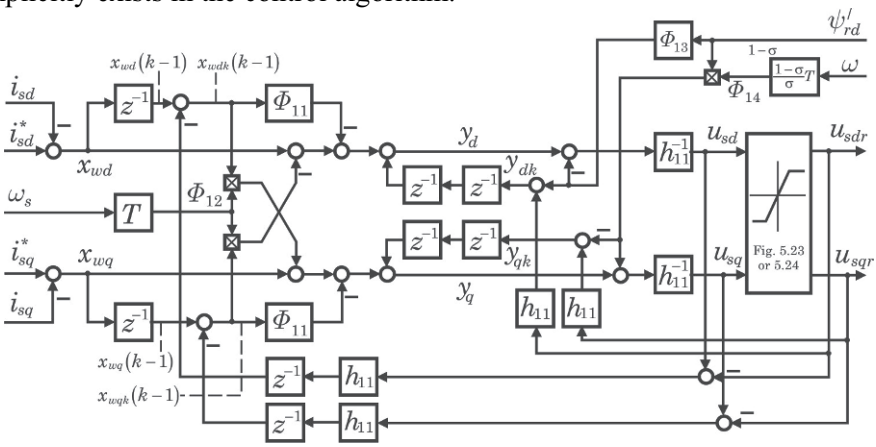

Fig. 5.25 Complete structure of the current vector controller with dead-beat-behaviour

To derive – the design in the chapter 5.3.1 serves as an example – the formula for the reverse correction, the equation (5.17) is re-written as follows:

$$\mathbf{y}(k) = \mathbf{H}\,\mathbf{u}_s(k+1) + \mathbf{h}\,\psi(k+1) \tag{5.81}$$

Assuming a largely constant rotor flux the following result will be obtained after substituting the equation (5.81) into (5.25):

$$\mathbf{H}\,\mathbf{u}_s(k) = \mathbf{x}_w(k-1) - \mathbf{\Phi}\,\mathbf{x}_w(k-2) + \mathbf{H}\,\mathbf{u}_s(k-2) \tag{5.82}$$

Assumed that the voltage goes into the limitation in time instant (k), i.e. instead of the voltage $\mathbf{u}_s(k)$ to be realized only $\mathbf{u}_{sr}(k)$ was realized, (5.82) turns into the equation (5.83).

$$\mathbf{H}\,\mathbf{u}_{sr}(k) = \mathbf{x}_{wc}(k-1) - \mathbf{\Phi}\,\mathbf{x}_w(k-2) + \mathbf{H}\,\mathbf{u}_s(k-2) \tag{5.83}$$

$\mathbf{x}_{wc}$ = Control errors corrected

$\mathbf{u}_{sr}$ = Voltage actually realized after limitation

The subtraction of the equations (5.82) and (5.83) produces for the corrected deviation:

$$\mathbf{x}_{wc}(k-1) = \mathbf{x}_w(k-1) - \mathbf{H}\left[\mathbf{u}_s(k) - \mathbf{u}_{sr}(k)\right] \tag{5.84}$$

Also the accumulated values $\mathbf{y}$ according to the equation (5.25) have to be corrected according to the equation (5.17) with the correct voltage values:

$$\mathbf{y}_k(k) = \mathbf{H}\,\mathbf{u}_{sr}(k+1) + \mathbf{h}\,\psi(k+1) \tag{5.85}$$

The formulae for the reverse correction for the designs with FAT behavior or for the additional integral controllers of the state space design can also be derived similarly. The figure 5.25 exemplarily illustrates the design with dead beat behaviour.

The implementation of the complete control algorithm in figure 5.25 is outlined by the program flowchart in figure 5.26.

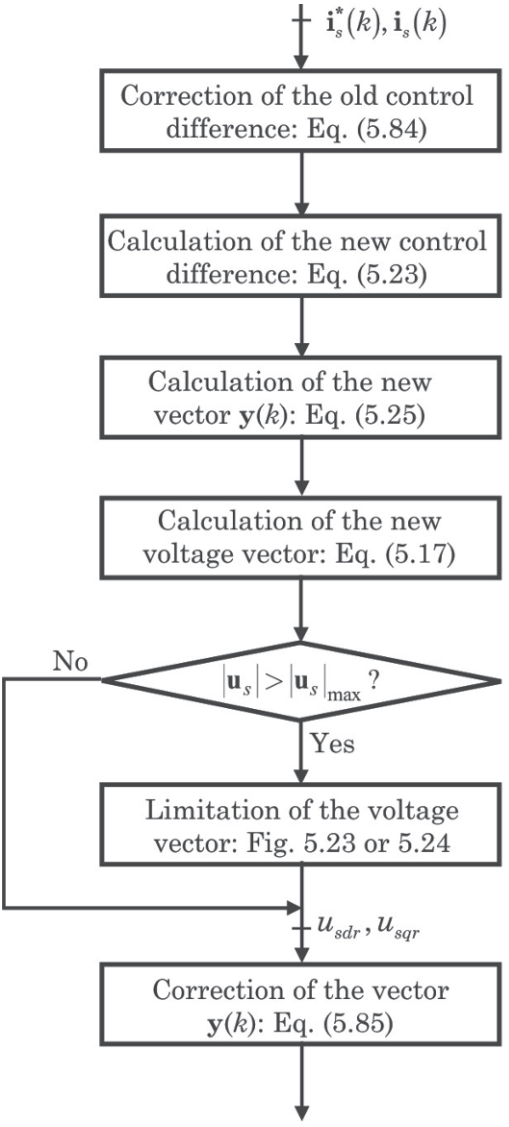

Fig. 5.26 Program flowchart of the current vector controller with dead beat behaviour

5.6 References

Brod DM, Novotny DN (1985) Current control of VSI-PWM inverters. IEEE Trans. on IA 21

Dittrich JA (1998) Anwendung fortgeschrittener Steuer- und Regelverfahren bei Asynchronantrieben. Habilitationsschrift, TU Dresden

Enjeti P, Lindsay JF, Ziogas PD, Rashid MH (1988) New current control scheme for PWM inverters. IEE Proceedings, Vol. 135, Pt.B, No. 4, July, pp. 172 – 179

Föllinger O (1982) Lineare Abtastsysteme. R. Oldenbourg Verlag: München Wien

Hofmann W (1984) Entwurf und Eigenschaften einer digitalen Vektorregelung von Asynchronmotoren mit gesteuertem Rotorfluß. Dissertation, TU Dresden

Holtz J, Stadtfeld S (1983) Fieldoriented control by forced motor currents in a voltage fed inverter drive. IFAC Symposium Control in Power Electronics an Electrical Drives, Lausanne, Switzerland, pp. 103 – 110

Holtz J, Stadtfeld S (1983) A predictive controller for the stator current vector of AC machines fed from a switched voltage source. IPEC Tokyo, Conf. Rec., pp. 1665 – 1675

Holtz J, Stadtfeld S (1985) A PWM inverter drive system with on-line optimized pulse patterns. EPE Brussel Conf. Rec., pp. 3.21 – 3.25

Isermann R (1987) Digitale Regelsysteme. Bd. 2, Springer Verlag: Berlin Heidelberg New York London Paris Tokyo

Kazmierkowski MP, Wojciak A (1988) Current control of VSI-PWM inverter-fed induction motor. Warsav Uni. of Technology, Institute of Control and Industrial Electronics, PE 7945

Kazmierkowski MP, Dzieniakowski MA, Sulkowski W (1988) Novel space vector based current controller for PWM-inverters. Summary, Warsav Uni. of Technology, Institute of Control and Industrial Electronics

Le-Huy H, Dessaint LA (1986) An adaptive current controller for PWM-inverters. IEEE PESC Conf., pp. 610 – 616

Malesani L, Tenti P (1987) A novel hysteresis control method for current controlled VSI-PWM inverters with constant modulation frequency. Conf. Rec. of IEEE-IAS Ann. Meet., pp. 851 – 855

Mayer HR (1988) Entwurf zeitdiskreter Regelverfahren für Asynchronmotoren unter Berücksichtigung der diskreten Arbeitsweise des Umrichters. Dissertation, Uni. Erlangen – Nürnberg

Meshkat S, Persson EK (1984) Optimum current vector control of brushless servo amplifier using microprocessors. IEEE IAS Ann. Meet. Conf. Rec., pp. 451 – 457

Nabae A, Oyasawara S, Akagi H (1985) A novel control scheme of current-controlled PWM inverters. IEEE – IAS Ann. Meet. Conf. Rec., pp. 473 – 478

Peak SC, Plunkett AB (1982) Transistorized PWM inverter-induction motor drive system. IEEE – IAS Ann. Meet. Conf. Rec., pp. 892 – 893

Pfaff G, Wick A (1983) Direkte Stromregelung bei Drehstromantrieben mit Pulswechselrichter. Regelungstechnische Praxis (rtp) 24, H. 11, S. 472 – 477

Quang NP (1990) Verfahren zur Stromregelung in Drehstromstellantrieben: Lösungsprinzipien und deren Grenzen. Fachtagung „Steuerung mechanischer Systeme“, TU Chemnitz, Februar, S. 102 – 105

Quang NP (1991) Schnelle Drehmomenteinprägung in Drehstromstellantrieben. Dissertation, TU Dresden

Quang NP (1994) Dokumentation zur Regelungssoftware mit TMS 320C25 von REFU 402Vectovar. REFU Elektronik GmbH, Abt. E1, interner Bericht

Quang NP (1996) Mehrgrößenregler löst PI-Regler ab: Von den Parametern zu programmierbaren Reglergleichungen. Elektronik, H.8, S. 112 – 120

Quang NP (1996) Digital Controlled Three-Phase Drives. Education Publishing House: Hanoi (book in vietnamese: Điều khiển tự động truyền động điện xoay chiều ba pha. Nhà xuất bản Giáo dục Hà Nội)

Quang NP, Schönfeld R (1991) Stromvektorregelung für Drehstromstellantriebe mit Pulswechselrichter. atp, Nov., S. 401 – 405 (msr)

Quang NP, Schönfeld R (1991) Stromzustandsregelung: Neues Konzept zur Ständerstromeinprägung für Drehstromstellantriebe mit Pulswechselrichter. atp, Dez., S. 432 – 436 (msr)

Quang NP, Schönfeld R (1993) Dynamische Stromregelung zur Drehmoment-einprägung in Drehstromantrieben mit Pulswechselrichter. Archiv für Elektrotechnik / Archiv of Electrical Engineering 76, S. 317 – 323

Quang NP, Schönfeld R (1993) Eine Stromvektorregelung mit endlicher Einstellzeit für dynamische Drehstromantriebe. Archiv für Elektrotechnik / Archiv of Electrical Engineering 76, S. 377 – 385

Rodriguez J, Kastner G (1987) Nonlinear current control of an inverter-fed induction machine. etz Archiv, Bd. 9, H. 8, S. 245 – 250

Rowan TM, Kerkman RJ, Lipo TA (1987) Operation of naturally sampled current regulators in the transition mode. IEEE Trans. on IA, IA- 23, No. 4, July/August, pp. 586 – 596

Schönfeld R, Krug H, Geitner GH, Stoev A (1985) Regelalgorithmen für digitale Regler von elektrischen Antrieben. msr, Berlin 28 H. 9, S. 390 – 394

Seifert D (1986) Stromregelung der Asynchronmaschine. etz Archiv, Bd. 6, H. 5, S. 151 – 156

Wiesing J (1994) Betrieb der feldorientiert geregelten Asynchronmaschine im Bereich oberhalb der Nenndrehzahl. Dissertation, Uni. Paderborn

Zhang J, Thiagarajan V, Grant T, Barton TH (1988) New approach to field orientation control of a CSI induction motor drive. IEE Proceedings, Vol. 135, Pt.B, No. 1, January, pp. 1 – 7